THE ASTROPHYSICAL JOURNAL, 333:848–872, 1988 October 15

THE DISCRETE-DIPOLE APPROXIMATION AND ITS APPLICATION TO INTERSTELLAR GRAPHITE GRAINS

B. T. DRAINE
Princeton University Observatory
Received 1988 February 2; accepted 1988 April 12

ABSTRACT

The discrete-dipole approximation for computing scattering and absorption by particles, originally developed by Purcell and Pennypacker, is a general method for computing scattering and absorption by a particle of arbitrary shape. Anisotropic dielectric functions and radiative reaction corrections are incorporated into the formalism of this method. An iterative algorithm for obtaining numerical solutions is employed which, unlike algorithms presented previously, works well for arbitrary complex dielectric functions. Validity criteria for the discrete-dipole approximation are discussed, including the importance of magnetic dipole effects and surface granularity. Discrete-dipole results for "spheres" with up to $N = 2320$ dipoles are compared with exact Mie theory calculations for two cases of the complex refractive index: $m = 1.7 + 0.1i$ and $m = 3 + 4i$; agreement is excellent within the expected domain of validity, although surface granularity limits the accuracy when the refractive index is large. The discrete dipole method is applied to examine the ultraviolet optical properties of particles composed of graphite, with its extremely anisotropic wavelength-dependent dielectric tensor. The optical properties of graphite spheres are computed, and compared to the usual "$\frac{1}{3}$–$\frac{2}{3}$" approximation based on Mie theory; it is found that the "$\frac{1}{3}$–$\frac{2}{3}$" approximation is surprisingly good, at least for the cases considered. Optical properties are computed for graphite cylinders with axial ratios ranging from 3:1 "disks" to 1.5:1 "rods," and equivalent radii up to $a_{eq} = 200$ Å. The 3:1 disks produce an extinction feature significantly longward of 2175 Å, and therefore can be ruled out as an appreciable component of the interstellar grain population. The 1.5:1 disks, and the 1.5:1 rods, produce an extinction feature which is similar enough to the observed 2175 Å feature that such grains cannot be rejected as a possible source of the observed 2175 Å feature. Cross sections for linear and circular dichroism have been computed; the 1.5:1 disks and the 1.5:1 rods have quite distinct polarization "signatures." If the 2175 Å extinction feature is due to graphite particles, and these particles are partially aligned, then observations of linear and circular polarization in the ultraviolet can be used to determine the particle shape.

Subject headings: interstellar: grains — polarization — radiative transfer

I. INTRODUCTION

Efforts to infer the size, morphology, and composition of interstellar dust in general rely on comparison between observations of extinction, absorption, scattering, or emission of electromagnetic radiation by dust, on the one hand, and theoretical models, on the other. Optical cross sections are required before the models can be computed for specific grain candidates.

Unfortunately, our ability to theoretically compute scattering and absorption cross sections for solid particles is extremely limited. If the particles are spherical, homogeneous, and isotropic, the rigorous solutions obtained by Mie (1908) and Debye (1909)—so-called "Mie scattering theory"—can be employed to compute any desired optical property of the grain provided only that the sphere is not extremely large compared to the wavelength. The observed polarization of starlight by the interstellar medium, however, manifestly requires that a significant fraction of the interstellar grains be appreciably nonspherical. Furthermore, some candidate grain materials—graphite, in particular—have anisotropic optical properties, so for these particles Mie theory would not be applicable even if the particles were to be homogeneous spheres. Finally, it is clear that in any case one would not expect typical interstellar grains—the result of complicated and sometimes violent processing—to be spherical.

For nonspherical particles, rigorous analytic scattering solutions exist only for special cases: particles very small compared to the wavelength, infinite cylinders, and, recently, homogeneous, isotropic spheroids (Asano and Yamamoto 1975; Asano 1979; Asano and Sato 1980; Onaka 1980). The reader is referred to the excellent book by Bohren and Huffman (1983) for a review of these solutions.

Several approaches have been followed to obtain absorption and scattering cross sections for finite nonspheroidal particles. The "T-matrix" technique involves an exact expansion of the exterior radiation field in terms of spherical harmonics; the expansion is truncated, and the expansion coefficients are determined numerically by casting the scattering problem in integral form. The T-matrix method has been applied to finite capped cylinders (Barber and Yeh 1975) and axisymmetric "T_n particles" (Wiscombe and Mugnai 1980). While the method can in principle be applied to homogeneous particles of arbitrary shape and size, it appears that considerable effort is involved in modifying the treatment for each new shape. Wiscombe and Mugnai reported difficulties with convergence of the method for great elongations or deep concavities, and remarked that the computational demands would be "prohibitive" for other than rotationally symmetric shapes. Perturbation theory has recently been applied to calculate scattering cross sections for finite cylinders (Haracz, Cohen, and Cohen 1984, 1985), but is restricted to objects which are small compared to the wavelength and to refractive indices

that are not too large. Wright (1987) has recently developed a method for calculating absorption cross section for grains modeled as aggregates of conducting spheres, but this approach is valid only in the long-wavelength limit.

Purcell and Pennypacker (1973) developed the "discrete dipole approximation" (henceforth DDA), a very flexible and general technique for calculating the optical properties of particles of arbitrary shapes. The DDA replaces the solid particle by an array of N point dipoles, with the spacing between the dipoles small compared to the wavelength. Each dipole has an oscillating polarization in response to both an incident plane wave and the electric fields due to all of the other dipoles in the array; the self-consistent solution for the dipole polarizations can be obtained as the solution to a set of coupled linear equations. Purcell and Pennypacker presented solutions with $N \leq 256$; they reported that under some circumstances they encountered difficulties with convergence of the iterative method they employed to obtain solutions. Shapiro (1975) subsequently used the DDA to calculate the optical properties of brick-shaped magnetite grains (with $N = 128$), using direct solution of the linear equations by matrix inversion, a method which unfortunately is feasible only for small values of N. The DDA was subsequently applied to inhomogeneous spheroids (with $N = 389$) by Druger *et al.* (1979) and was used (with $N = 64$) by Kattawar and Humphreys (1980) to compute scattering from two neighboring spheres. Yung (1978), using a new iterative method to solve the linear equations, calculated cross sections for spheres with N as large as 15,600. Unfortunately, however, the algorithm presented by Yung fails to converge for grains with strongly absorptive refractive indices. Most recently, Singham and Bohren (1987) have presented a new iterative approach for obtaining numerical solutions to the DDA scattering problem.

In § II of the present paper, the DDA is reviewed, and corrections for radiative reaction are incorporated into the formalism. Formulae used to extract the desired cross sections from a discrete-dipole solution are presented in § III. Validity criteria for the DDA are examined in § IV, resulting in two validity criteria (eqs. [4.01], [4.05]). Section V describes an iterative algorithm, based on the method of conjugate gradients, which has been found to consistently converge on solutions to the system of complex linear equations, for absorptive as well as nonabsorptive dielectric functions. The accuracy of the DDA is assessed in § VI by comparing calculations for discrete-dipole representations of spheres with exact results from Mie theory. Cross sections for graphite spheres are computed in § VII and are compared to the often-used "$\frac{1}{3}$–$\frac{2}{3}$" approximation. In § VIII, extinction cross sections are presented for nonspherical graphite grains, and comparison is made to the observed interstellar 2175 Å extinction feature. A summary of the principal results is presented in § IX.

II. THE DISCRETE DIPOLE MODEL

a) *Dipole Polarizabilities: Effects of Radiative Reaction*

Following Purcell and Pennypacker the individual dipoles will be located on a simple cubic lattice. Let the index $j = 1, \ldots, N$ run over the occupied lattice sites. Each dipole j is characterized by a (symmetric) polarizability tensor α_j, such that $\boldsymbol{P}_j = \alpha_j \boldsymbol{E}_{\text{ext},j}$, where $\boldsymbol{P}_j$ is the instantaneous (complex) dipole moment of dipole j, and $\boldsymbol{E}_{\text{ext},j}$ is the instantaneous (complex) electric field at position j due to all sources external to j: i.e., $\boldsymbol{E}_{\text{ext},j}$ is the electric field at position j due to the radiation incident on the grain plus the other $N - 1$ oscillating dipoles.

If the grain material is isotropic, then the polarizability tensor is diagonal with equal components $\alpha_{j,xx} = \alpha_{j,yy} = \alpha_{j,zz}$; in other words, α_j may be treated as a scalar quantity.

If the grain material is anisotropic, the polarizability tensor is not proportional to the identity matrix. For any individual dipole, it is possible to choose a Cartesian coordinate system such that α is diagonalized, with diagonal elements $\alpha_{j,xx}$, $\alpha_{j,yy}$, and $\alpha_{j,zz}$. If the grain material is monocrystalline (and therefore homogeneous), then the dielectric tensor ϵ is independent of position within the grain, and a coordinate system can be chosen in which ϵ is diagonalized, with diagonal elements ϵ_{ll}; each of the individual dipole polarizability tensors α_j will also be diagonal in this coordinate system, with diagonal elements $\alpha_{j,ll}$. In this paper we will restrict attention to the case where a coordinate system can be chosen in which the dielectric tensor, even if inhomogeneous, is diagonal, so that all of the individual dipole polarizability tensors can be simultaneously diagonalized. It is straightforward, although notationally tedious, to generalize to the case where the dipoles may have nondiagonal polarizability tensors.

The question of what polarizability tensor α_j to adopt for each individual dipole is nontrivial. Purcell and Pennypacker used the Clausius-Mossotti relation to obtain an estimate α_j^0 for the polarizability:

$$\alpha_{j,ll}^0 = \frac{3}{4\pi n}\frac{\epsilon_{ll} - 1}{\epsilon_{ll} + 2}, \tag{2.01}$$

where n is the number density of dipoles. For polarizable point dipoles located on a cubic lattice, this relation is exact in the zero-frequency limit (see, e.g., Purcell 1965, pp. 333–338; Kittel 1971; Jackson 1975), but is not exact at finite frequencies. To see why it fails, consider a nonabsorptive material with real ϵ, in which case equation (2.01) would imply real α; however, a single such dipole irradiated by a plane wave would scatter, and therefore attenuate, the plane wave, and this attentuation requires that α have an imaginary component in order that the oscillating dipole not be exactly in phase with the incident plane wave.[1] Since we will be considering only periodic electric fields, it is straightforward to allow for the "radiative reaction" by assuming that, in addition to the electric fields due to other sources, each dipole is exposed to a "radiative reaction" electric field $\boldsymbol{E}_{\text{rad},j} = (\frac{2}{3})ik^3\boldsymbol{P}_j$ (Jackson 1975), in which case

$$\boldsymbol{P}_j = \alpha_j \boldsymbol{E}_{\text{ext},j} = \alpha_j^0(\boldsymbol{E}_{\text{ext},j} + \boldsymbol{E}_{\text{rad},j}), \tag{2.02}$$

which implies a polarizability (now assuming that the coordinate system is chosen so that α_j^0 is diagonalized)

$$\alpha_{j,ll} = \frac{\alpha_{j,ll}^0}{1 - (2/3)ik^3\alpha_{j,ll}^0} = \alpha_{j,ll}^0\left[1 - \frac{2i}{3N}(ka_{\text{eq}})^3\frac{\epsilon_{ll} - 1}{\epsilon_{ll} + 2}\right]^{-1}, \tag{2.03}$$

where the "equivalent radius" $a_{\text{eq}} \equiv (3N/4\pi n)^{1/3}$ is the radius of a sphere containing the same number of dipoles. Our result (eq. [2.03]) for the polarizability differs from equation (2.01) only through the term proportional to $(ka_{\text{eq}})^3/N$, which clearly vanishes in the zero frequency limit ($ka_{\text{eq}} \to 0$) or the continuum limit ($N \to \infty$). This "radiative reaction" correction will generally be a minor one in those cases where the discrete

[1] It is easily seen from the optical theorem that the forward scattering amplitude must have an imaginary component if the dipole scatters power out of the beam; this implies that the polarizability must have an imaginary component.

dipole model provides a good approximation; however, it is an important point of principle, since otherwise the optical theorem is violated and cannot be used to evaluate the total extinction cross section for the grain.

b) *Formulation of the General Scattering Problem*

It is desired to obtain a self-consistent set of dipole moments $\boldsymbol{P}_j$ $(j = 1, \ldots, N)$ so that $\boldsymbol{P}_j = \alpha_j \boldsymbol{E}_{\text{ext},j}$. As noted by Purcell and Pennypacker (1973) and Yung (1978), this can be rewritten as N simultaneous complex vector equations of the form

$$\boldsymbol{P}_j = \alpha_j \left(\boldsymbol{E}_{\text{inc},j} - \sum_{k \neq j} \mathbf{A}_{jk} \boldsymbol{P}_k \right) , \tag{2.04}$$

where $\boldsymbol{E}_{\text{inc},j}$ is the electric field at position j due to the incident plane wave,

$$\boldsymbol{E}_{\text{inc},j} = \boldsymbol{E}_0 \exp (i\boldsymbol{k} \cdot \boldsymbol{r}_j - i\omega t) , \tag{2.05}$$

and $-\mathbf{A}_{jk} \boldsymbol{P}_k$ is the contribution to the electric field at position j due to the dipole at position k:

$$\mathbf{A}_{jk} \boldsymbol{P}_k = \frac{\exp (ikr_{jk})}{r_{jk}^3} \left\{ k^2 \boldsymbol{r}_{jk} \times (\boldsymbol{r}_{jk} \times \boldsymbol{P}_k) + \frac{(1 - ikr_{jk})}{r_{jk}^2} \times \left[r_{jk}^2 \boldsymbol{P}_k - 3\boldsymbol{r}_{jk} (\boldsymbol{r}_{jk} \cdot \boldsymbol{P}_k) \right] \right\} \quad (j \neq k) , \tag{2.06}$$

where $\boldsymbol{r}_{jk} \equiv \boldsymbol{r}_j - \boldsymbol{r}_k$. Equation (2.06) serves to define the matrices $\mathbf{A}_{jk}$ for $j \neq k$. It is convenient to define also matrices

$$\mathbf{A}_{jj} = \alpha_j^{-1} , \tag{2.07}$$

so that the scattering problem can be compactly formulated as a set of N inhomogeneous linear complex vector equations:

$$\sum_{k=1}^{N} \mathbf{A}_{jk} \boldsymbol{P}_k = \boldsymbol{E}_{\text{inc},j} \quad (j = 1, \ldots, N) . \tag{2.08}$$

It is easy to show that the 3×3 matrices $\mathbf{A}_{jk}$ are symmetric: $(\mathbf{A}_{jk})_{lm} = (\mathbf{A}_{jk})_{ml}$.

It is further convenient to define two $3N$-dimensional vectors $\tilde{\mathbf{P}} = (\boldsymbol{P}_1, \boldsymbol{P}_2, \ldots, \boldsymbol{P}_N)$ and $\tilde{\mathbf{E}}_{\text{inc}} = (\boldsymbol{E}_{\text{inc},1}, \boldsymbol{E}_{\text{inc},2}, \ldots, \boldsymbol{E}_{\text{inc},N})$, and a $3N \times 3N$ symmetric matrix $\tilde{\mathbf{A}}$ such that $\tilde{\mathbf{A}}_{3j-l,3k-m} = (\mathbf{A}_{jk})_{3-l,3-m}$, so that the problem is reduced to a single matrix equation:

$$\tilde{\mathbf{A}} \tilde{\mathbf{P}} = \tilde{\mathbf{E}}_{\text{inc}} . \tag{2.09}$$

A variety of techniques, including direct inversion of the matrix $\tilde{\mathbf{A}}$, are available for solving for the unknown vector $\tilde{\mathbf{P}}$. The method used in this paper is discussed below in § V.

c) *Grains with Fourfold Symmetry*

Solution of the general scattering problem requires solution of $3N$ simultaneous linear equations. This is extremely time-consuming for large values of N. In the case of scattering problems with appropriate symmetries, the problem can be simplified if the symmetry can be exploited to reduce the number of unknowns. Here we consider the special case of radiation incident along the x-axis, linearly polarized along the y-axis, with the target grain having reflection symmetry through the x-y and x-z planes. We will assume that the dipoles from which the grain is constructed do not lie on the x-y or x-z planes, and are located at positions which are symmetric with respect to reflection through the x-y or x-z planes [i.e., if a dipole is located at location (x, y, z), then there are other dipoles (having the same polarizability tensor α) at locations $(x, y, -z)$, $(x, -y, z)$, and $(x, -y, -z)$].

With this symmetry the number of dipoles which must be solved for is only $N/4$, since the knowledge of the polarization at (x, y, z) can be used to determine the polarization at three other positions: $(x, -y, z)$, $(x, -y, -z)$, and $(x, y, -z)$:

$$P_x(x, y, z) = -P_x(x, -y, z) = -P_x(x, -y, -z) = P_x(x, y, -z) , \tag{2.10a}$$

$$P_y(x, y, z) = P_y(x, -y, z) = P_y(x, -y, -z) = P_y(x, y, -z) , \tag{2.10b}$$

$$P_z(x, y, z) = -P_z(x, -y, z) = P_z(x, -y, -z) = -P_z(x, y, -z) . \tag{2.10c}$$

It is straightforward to use the elements of the above-defined $3N \times 3N$ matrix $\tilde{\mathbf{A}}$ to obtain a $(3N/4) \times (3N/4)$ symmetric matrix $\mathbf{B}$ such that the scattering problem is reduced to solving

$$\mathbf{B} \tilde{\mathbf{P}}' = \tilde{\mathbf{E}}'_{\text{inc}} , \tag{2.11}$$

where $\tilde{\mathbf{P}}'$ consists of only the $N/4$ dipole moments $\boldsymbol{P}_j$ lying in the quadrant $y > 0$, $z > 0$, and $\tilde{\mathbf{E}}'_{\text{inc}}$ consists of the incident electric field vectors at those positions. This reduction of the number of equations by a factor of 4 can easily reduce the amount of computing by an order of magnitude or more (in the case of solution by direct matrix inversion, the computing would be reduced by a factor $4^3 = 64$). The storage requirements are also somewhat eased.

III. CROSS SECTIONS

a) *Extinction*

Once the polarizations $\boldsymbol{P}_j$ are known, the extinction cross section for the grain is computed from the forward-scattering amplitude using the optical theorem:

$$C_{\text{ext}} = \frac{4\pi k}{|\boldsymbol{E}_{\text{inc}}|^2} \sum_{j=1}^{N} \text{Im} (\boldsymbol{E}^*_{\text{inc},j} \cdot \boldsymbol{P}_j) . \tag{3.01}$$

This result is equivalent to the expression given by Purcell and Pennypacker.[2] The relationship between the extinction cross section and the forward scattering amplitudes is given in equation (3.17) below.

b) *Absorption*

The absorption cross section is obtained by summing over the rate of energy dissipation by each of the dipoles. To obtain an expression for the rate of energy dissipation by an individual dipole, it is simplest to first contemplate an isolated point dipole at $\boldsymbol{r} = 0$ irradiated by an incident plane wave. The dipole polarization is simply $\boldsymbol{P} = \alpha \boldsymbol{E}_{\text{inc}}$. The extinction cross section is readily obtained from the optical theorem (above eq. [3.01]):

$$C_{\text{ext}} = \frac{4\pi k}{|\boldsymbol{E}_{\text{inc}}|^2} \text{Im} (\boldsymbol{E}^*_{\text{inc}} \cdot \alpha \boldsymbol{E}_{\text{inc}}) \tag{3.02}$$

(for an isotropic polarizability, this reduces to $C_{\text{ext}} =$

[2] Except for a difference in sign: their expression applies for the convention $\boldsymbol{E}_{\text{inc}} \propto \exp (i\omega t - i\boldsymbol{k} \cdot \boldsymbol{r})$, whereas we assume $\boldsymbol{E}_{\text{inc}} \propto \exp (i\boldsymbol{k} \cdot \boldsymbol{r} - i\omega t)$.

$4\pi k$ Im α). Thus the rate at which energy is removed from the incident beam is

$$\left(\frac{dE}{dt}\right)_{\rm ext} = \frac{\omega}{2}\,{\rm Im}\,(\boldsymbol{E}^*\cdot\boldsymbol{P}) = \frac{\omega}{2}\,{\rm Im}\,[\boldsymbol{P}\cdot(\alpha^{-1})^*\boldsymbol{P}^*]\,. \quad (3.03)$$

Since the power radiated by the oscillating dipole is

$$\left(\frac{dE}{dt}\right)_{\rm sca} = \frac{\omega^4}{3c^3}\,\boldsymbol{P}\cdot\boldsymbol{P}^*\,, \quad (3.04)$$

it follows that the rate at which energy is absorbed is

$$\left(\frac{dE}{dt}\right)_{\rm abs} = \frac{\omega}{2}\left\{{\rm Im}\,[\boldsymbol{P}\cdot(\alpha^{-1})^*\boldsymbol{P}^*] - \frac{2}{3}\,k^3\boldsymbol{P}\cdot\boldsymbol{P}^*\right\}. \quad (3.05)$$

This differs from the expression of Purcell and Pennypacker due to the presence of the term proportional to k^3, which must be included in order to self-consistently include the effects of radiative reaction. Thus the absorption cross section for the entire grain is

$$C_{\rm abs} = \frac{4\pi k}{|\boldsymbol{E}_{\rm inc}|^2}\sum_{j=1}^{N}\left\{{\rm Im}\,[\boldsymbol{P}_j\cdot(\alpha_j^{-1})^*\boldsymbol{P}_j^*] - \frac{2}{3}\,k^3\boldsymbol{P}_j\cdot\boldsymbol{P}_j^*\right\}. \quad (3.06)$$

c) *Scattering*

The scattering cross section can in principle be obtained from the difference of the extinction and absorption cross sections: $C_{\rm sca} \equiv C_{\rm ext} - C_{\rm abs}$. When absorption is dominant, this requires that $C_{\rm ext}$ and $C_{\rm abs}$ be computed to high accuracy. Since the method of computation is iterative, it may be costly (and perhaps even numerically infeasible) to obtain the solution vectors $\boldsymbol{P}_j$ to the necessary degree of accuracy. It is, of course, possible to compute the scattering cross section directly by computing the power radiated by the array of oscillating dipoles:

$$C_{\rm sca} = \frac{k^4}{|\boldsymbol{E}_{\rm inc}|^2}\int d\Omega\left|\sum_{j=1}^{N}[\boldsymbol{P}_j - \hat{\boldsymbol{n}}(\hat{\boldsymbol{n}}\cdot\boldsymbol{P}_j)]\exp(-ik\hat{\boldsymbol{n}}\cdot\boldsymbol{r}_j)\right|^2, \quad (3.07)$$

where $\hat{\boldsymbol{n}}$ is a unit vector in the direction of scattering, and $d\Omega$ is the element of solid angle. It is often also of interest to evaluate the scattering asymmetry parameter

$$g \equiv \langle\cos\theta\rangle = \frac{k^3}{C_{\rm sca}|\boldsymbol{E}_{\rm inc}|^2}\int d\Omega\,\hat{\boldsymbol{n}}\cdot\boldsymbol{k}\left|\sum_{j=1}^{N}[\boldsymbol{P}_j - \hat{\boldsymbol{n}}(\hat{\boldsymbol{n}}\cdot\boldsymbol{P}_j)] \times\exp(-ik\hat{\boldsymbol{n}}\cdot\boldsymbol{r}_j)\right|^2. \quad (3.08)$$

d) *Phase Lag*

In addition to the cross sections for attenuation and scattering, it is of interest to know how the phase of the wave propagated through a dust medium is changed relative to the phase it would have had if propagating *in vacuo*. The phase-lag cross section is defined in terms of the imaginary component of the forward-scattering amplitude, and is here defined so that the phase lag (in radians) after propagating a distance L is just $n_{\rm gr}C_{\rm pha}L$, where $n_{\rm gr}$ is the number density of grains.[3] With this definition, we have

$$C_{\rm pha} = \frac{2\pi k}{|\boldsymbol{E}_{\rm inc}|^2}\sum_{j=1}^{N}{\rm Re}\,[\boldsymbol{E}_{{\rm inc},j}^*\cdot\boldsymbol{P}_j]\,. \quad (3.09)$$

Note that the present definition of $C_{\rm pha}$ is a factor of 2 smaller than the definition of Martin (1972).

e) *Linear and Circular Dichroism*

Differential extinction between two orthogonal polarizations will produce linear polarization; the "polarization cross section" is defined to be

$$C_{\rm pol} \equiv C_{\rm ext}(\boldsymbol{E}_0\|\hat{\boldsymbol{e}}) - C_{\rm ext}(\boldsymbol{E}_0\perp\hat{\boldsymbol{e}})\,, \quad (3.10)$$

where $\hat{\boldsymbol{e}}$ is a unit vector perpendicular to the direction of propagation, chosen so that $C_{\rm ext}$ is maximized or minimized for $\boldsymbol{E}_0\|\hat{\boldsymbol{e}}$. Differential phase lag between two orthogonal polarizations will convert linear polarization into circular polarization; accordingly we define the circular polarization cross section $C_{\rm cpol}$ to be

$$C_{\rm cpol} \equiv C_{\rm pha}(\boldsymbol{E}_0\|\hat{\boldsymbol{e}}) - C_{\rm pha}(\boldsymbol{E}_0\perp\hat{\boldsymbol{e}})\,. \quad (3.11)$$

In a medium where the direction of grain alignment rotates along the line of sight, initially unpolarized light will acquire a degree of circular polarization proportional to the product of $C_{\rm pol}$ and $C_{\rm cpol}$ (Martin 1972).

f) *Results for Arbitrary Incident Polarization*

Absorption, scattering, and extinction cross sections will generally depend upon the polarization state of the incident wave. Here we present formulae which permit one to compute these cross sections for an arbitrary incident polarization, given results for any two orthogonal incident polarizations. Thus the scattering problem need be solved only twice for any particular direction of propagation.

Let $\hat{\boldsymbol{n}}_0$ be a unit vector in the direction of propagation of the incident radiation, and let $\hat{\boldsymbol{e}}_{01}$ and $\hat{\boldsymbol{e}}_{02} = \hat{\boldsymbol{n}}_0\times\hat{\boldsymbol{e}}_{01}$ be unit vectors ($\hat{\boldsymbol{e}}_{0m}^*\cdot\hat{\boldsymbol{e}}_{0n} = \delta_{mn}$) specifying two orthogonal polarization states for the incident wave. Now suppose that the scattering problem has previously been solved for each of the two polarizations $\hat{\boldsymbol{e}}_{01}$, $\hat{\boldsymbol{e}}_{02}$; let $\boldsymbol{P}_j^{(l)}$ represent the computed polarization of dipole j for an incident electric field $\boldsymbol{E}_{\rm inc} = E_0\hat{\boldsymbol{e}}_l\exp(ik\hat{\boldsymbol{n}}_0\cdot\boldsymbol{r} - i\omega t)$, and define $\boldsymbol{p}_j^{(l)} \equiv E_0^{-1}e^{i\omega t}\boldsymbol{P}_j^{(l)}$. The scattering properties of the particle may be fully characterized by a dimensionless 2×2 complex matrix $f_{ml}(\hat{\boldsymbol{n}}_0, \hat{\boldsymbol{n}})$, for scattering from incident direction $\hat{\boldsymbol{n}}_0$ and polarization vector $\hat{\boldsymbol{e}}_l$ into direction $\hat{\boldsymbol{n}}$ and polarization vector $\hat{\boldsymbol{e}}_m$, where

$$f_{ml}(\hat{\boldsymbol{n}}_0, \hat{\boldsymbol{n}}) \equiv k^3\sum_{j=1}^{N}\boldsymbol{p}_j^{(l)}\cdot\boldsymbol{e}_m^*\exp(-ik\hat{\boldsymbol{n}}\cdot\boldsymbol{r}_j)\,. \quad (3.12)$$

For an arbitrary incident wave

$$\boldsymbol{E}_{\rm inc} = \boldsymbol{E}_0\exp(ik\hat{\boldsymbol{n}}_0\cdot\boldsymbol{r} - i\omega t) = E_0\exp(ik\hat{\boldsymbol{n}}_0\cdot\boldsymbol{r} - i\omega t)\sum_{l=1}^{2}a_l\hat{\boldsymbol{e}}_{0l}\,, \quad (3.13)$$

where

$$E_0 \equiv (\boldsymbol{E}_0\cdot\boldsymbol{E}_0^*)^{1/2}\,, \quad (3.14)$$

$$a_l \equiv E_0^{-1}\boldsymbol{E}_0\cdot\hat{\boldsymbol{e}}_{0l}^*\,, \quad (3.15)$$

the scattered radiation with direction of propagation $\hat{\boldsymbol{n}}$ is given

[3] "Phase lag" is taken to be positive when the arrival time of a surface of constant phase is delayed relative to its arrival time *in vacuo*.

(in the radiation zone) by

$$\boldsymbol{E} = \frac{E_0}{kr} \exp\,(ik\hat{\boldsymbol{n}} \cdot \boldsymbol{r} - i\omega t) \sum_{m=1}^{2} \hat{\boldsymbol{e}}_m \sum_{l=1}^{2} f_{ml} a_l \,. \tag{3.16}$$

The extinction cross section may be obtained from the forward scattering amplitudes:

$$C_{\rm ext} = 4\pi k^{-2} \left\{ \sum_{l=1}^{2} |a_l|^2 \,\mathrm{Im}\, f_{ll}(0) + \mathrm{Im}[a_2 a_1^* f_{12}(0) + a_1 a_2^* f_{21}(0)] \right\}, \tag{3.17}$$

where $f_{ml}(0) \equiv f_{ml}(\hat{\boldsymbol{n}}_0, \hat{\boldsymbol{n}}_0)$, and for the forward direction we naturally adopt $\hat{\boldsymbol{e}}_m = \hat{\boldsymbol{e}}_{0m}$. The absorption cross section is

$$C_{\rm abs} = 4\pi k \sum_{j=1}^{N} \sum_{l=1}^{2} \sum_{m=1}^{2} \{\mathrm{Im}\,[a_l a_m^* \boldsymbol{p}_j^{(l)} \cdot (\alpha_j^{-1})^* \boldsymbol{p}_j^{(m)*}] - \tfrac{2}{3} k^3 a_l a_m^* \boldsymbol{p}_j^{(l)} \cdot \boldsymbol{p}_j^{(m)*}\} \,. \tag{3.18}$$

The differential scattering cross section into polarization state $\hat{\boldsymbol{e}}_n$ is

$$\left(\frac{dC_{\rm sca}}{d\Omega}\right)_n = k^{-2} \sum_{l=1}^{2} \sum_{m=1}^{2} a_l a_m^* f_{nl} f_{nm}^* \,, \tag{3.19}$$

and the total scattering cross section may be obtained by quadrature:

$$C_{\rm sca} = k^{-2} \sum_{l=1}^{2} \sum_{m=1}^{2} a_l a_m^* \sum_{n=1}^{2} \int d\Omega f_{nl} f_{nm}^* \,. \tag{3.20}$$

Finally, the phase-lag cross section is given by

$$C_{\rm pha} = 2\pi k^{-2} \left\{ \sum_{l=1}^{2} |a_l|^2 \,\mathrm{Re}\, f_{ll}(0) + \mathrm{Re}\,[a_2 a_1^* f_{12}(0) + a_1 a_2^* f_{21}(0)] \right\}. \tag{3.21}$$

Note that if one chooses $\hat{\boldsymbol{e}}_{01}$ and $\hat{\boldsymbol{e}}_1$ to lie in the scattering plane (corresponding to the standard definition of the "parallel" polarization state), then our unit vectors $\hat{\boldsymbol{e}}_{02} \equiv \hat{\boldsymbol{n}}_0 \times \hat{\boldsymbol{e}}_{01}$, $\hat{\boldsymbol{e}}_2 \equiv \hat{\boldsymbol{n}} \times \hat{\boldsymbol{e}}_1$ are opposite in sign to the convention adopted by Bohren and Huffman (1983 for the "perpendicular" polarization state, and our matrix elements f_{ml} are related to the "amplitude scattering matrix" S of Bohren and Huffman by

$$f_{11} = iS_2 \,, \tag{3.22a}$$

$$f_{12} = -iS_3 \,, \tag{3.22b}$$

$$f_{21} = -iS_4 \,, \tag{3.22c}$$

$$f_{22} = iS_1 \,. \tag{3.22d}$$

IV. VALIDITY CRITERIA

a) *Granularity of the Surface*

Consider a grain of volume V, represented by an array of N discrete dipoles. It will be useful to characterize the physical size of the grain by the "equivalent radius" $a_{\rm eq} \equiv (3V/4\pi)^{1/3}$, the radius of a sphere of equal volume. The nearest-neighbor distance between dipoles is $d = (4\pi/3N)^{1/3} a_{\rm eq}$. For a discrete-dipole model to provide a good approximation to the grain, it is necessary for N to be large enough (d small enough compared to $a_{\rm eq}$) that the boundary of the cubic array satisfactorily approximates the desired grain shape. The degree to which this surface granularity leads to numerical inaccuracy depends upon the value of the dielectric function, as will be seen below. Since the required computing varies approximately as $\sim N^2$, one wishes to select a value of N which is a local minimum of some measure $f(N)$ of the surface irregularity. The choice of a measure $f(N)$ is somewhat arbitrary. To measure departures from sphericity, we imagine placing a cube of volume d^3 at each occupied lattice site, and compute

$$f(N) \equiv (5/3)(4\pi/3)^{2/3} N^{-5/3} \sum_{i=1}^{N} (x_i^2 + y_i^2 + z_i^2 + d^2/12) \,;$$

$[f(N)]^{1/2} > 1$ is then the ratio of the radius of gyration to that of a perfect sphere of equal volume. For arrays symmetric about the origin, with dipoles located at positions $(x, y, z) = (i + \frac{1}{2}, j + \frac{1}{2}, k + \frac{1}{2})d$ (where i, j, k are integers), "good" values of N for approximating a sphere are $N = 136$, 160, 304, 672, 1064, 1640, 1904, 2320, ...; these values of N minimize the above choice of $f(N)$. Four such pseudospheres are shown in Figure 1.

To see how the surface granularity affects the accuracy of the calculations, we have calculated[4] the polarization of various discrete dipole "spheres" in the long-wavelength limit $ka_{\rm eq} \ll 1$, for an applied external electric field $\boldsymbol{E}_0 = E_0 \hat{\boldsymbol{y}}$; recall that a homogeneous ($N \to \infty$) sphere would have a uniform interior polarization $(3/4\pi)(\epsilon - 1)(\epsilon + 2)^{-1} \boldsymbol{E}_0$. In Figures 2*a* and 2*b* we show slices through $m = 1.7 + 0.1i$ ($\epsilon = 2.88 + 0.34i$) "spheres" consisting of $N = 136$ and $N = 1064$ dipoles. Results for $m = 3 + 4i$ ($\epsilon = -7 + 24i$) are shown in Figures 2*c* and 2*d*. In each case we show a "slice" through the grain along the $z = d/2$ plane. The arrows centered on each of the dipole sites lying in this plane show the direction and magnitude of the polarization projected onto the xy-plane. The scale is chosen so that if a dipole had the polarization $\boldsymbol{P}_\infty = (3d^3/4\pi)(\epsilon - 1)(\epsilon + 2)^{-1} \boldsymbol{E}_0$ expected in the limit $N \to \infty$ the arrow representing that polarization would have a length equal to the diameter d of the circles centered on each dipole. For the $N = 136$ models, it is evident that the polarization vectors are not purely in the y direction, as they would be for $N \to \infty$. This is apparently due mainly to the sharp "corners" of the cubic array—the deviations from the ideal sphere $\boldsymbol{P}_\infty$ appear to be largest near these corners. This effect is also present, although of a smaller magnitude, in the $N = 1064$ models. It is further seen that for the $N = 136$ models, most of the polarization vectors are in fact significantly larger than P_∞; this effect, which is most prominent in the $m = 3 + 4i$ case, presumably occurs because each dipole is less effectively "screened" from the external field E_0 than it would be if located within an $N = \infty$ sphere, for which the interior electric field is smaller than the external field by a factor $3/(\epsilon + 2)$. Note that the case $m = 3 + 4i$ considered here is one where quite strong screening is expected, since $|3/(\epsilon + 2)| = 0.1224$. With most of the polarization vectors significantly larger than P_∞, the absorption cross section of the $m = 3 + 4i$, $N = 136$ array exceeds that of the corresponding sphere by a factor 1.45.

For the $N = 1064$ shown in Figure 2*b*, it is seen that the interior polarization is more uniform, and closer in magnitude to the continuum limit. Nevertheless, even with $N = 1064$ the mean polarization exceeds P_∞ (and the absorption cross section exceeds that of a sphere) by a factor 1.22. Empirically, it appears as though the error (in the zero-frequency limit) scales

[4] The solutions shown were actually obtained using the general method described in § V below, with $ka = 10^{-6}$.

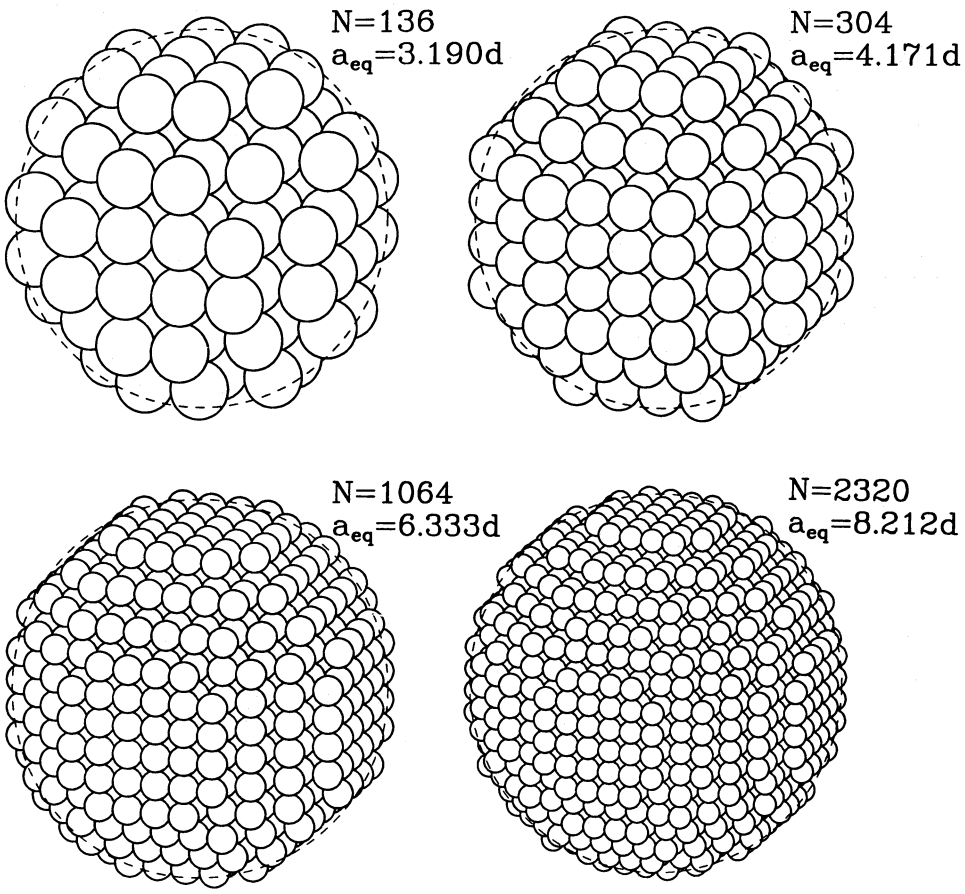

FIG. 1.—"Spherical" discrete dipole arrays considered in this paper, with $N = 136$, 304, 1064, and 2320

approximately as $N^{-1/3}$, consistent with the error being associated with the granularity of the surface. On the basis of a limited number of numerical calculations for spheres, we estimate that in order to attain a fractional error less than Δ (in the zero-frequency limit) the particle should satisfy the criterion

$$N > N_{\rm min} \approx 60|m-1|^3(\Delta/0.1)^{-3} . \quad (4.01)$$

This estimate for $N_{\rm min}$ applies to spheres; $N_{\rm min}$ for other convex shapes will differ by factors of order unity. The strong dependence on $|m-1|$ implies that discrete dipole calculations for materials with large refractive indices must either accept relatively large fractional errors Δ, or else employ very large values of N.

b) Granularity versus Wavelength and Skin Depth

A second necessary condition for the dipole array to provide an accurate representation of a homogeneous grain is that the length scale for variation of the electric field within the grain must be large compared to d. For specified $ka_{\rm eq}$ and refractive index m, it is useful to have a criterion with which to estimate how large N must be in order for the discrete dipole model to provide an accurate approximation.

In their discrete-dipole calculation of scattering by a sphere with $N = 136$, Purcell and Pennypacker note that appreciable inaccuracy (errors of more than $\sim 10\%$ in $Q_{\rm ext}$) occurs when $kd \gtrsim 1$. Yung (1978) states that it is necessary that $kd \lesssim \frac{1}{3}$ in order to obtain reliable results. It seems clear that the validity criterion should also depend upon the complex refractive index m of the material. One necessary condition is that d be small not just compared to the wavelength *in vacuo* $2\pi/k$ but also with the wavelength $2\pi/{\rm Re}(m)k$ within the material. In the event that the material is absorptive, a second necessary condition is that d be small compared to the attenuation length (or "skin depth") $2\pi/{\rm Im}(m)k$ for the electromagnetic wave. A simple criterion suggests itself: $kd|m| < \beta$, where β is some constant of order unity; obviously the value of β will depend on the desired degree of accuracy. Based on our calculations for $m = 1.7 + 0.1i$ (see § VI) we estimate the dimensionless factor $\beta \approx 1.0(\Delta/0.1)$, where Δ is the desired fractional accuracy. One thus obtains a condition on N:

$$N \gtrsim \frac{4\pi}{3}(ka_{\rm eq})^3|m|^3\left(\frac{\Delta}{0.1}\right)^{-3} . \quad (4.02)$$

As expected, large values of N will be required to compute scattering for large values of $ka_{\rm eq}$, or for materials (such as conductors) with large values of $|m|$.

c) Granularity: Neglect of Magnetic Dipole Absorption

The above criterion (4.02) is necessary but, as we shall see, not sufficient. The discrete dipole method replaces a cubic volume of grain material, of volume d^3, by a point *electric* dipole—magnetic (dipole) effects are neglected. Even for nonmagnetic materials, however, the induced magnetic moment associated with volume d^3 of grain material may not be negligible if the material is sufficiently conductive. In particular, "magnetic dipole" absorption may be comparable to, or greater than, the "electric dipole" absorption of equation

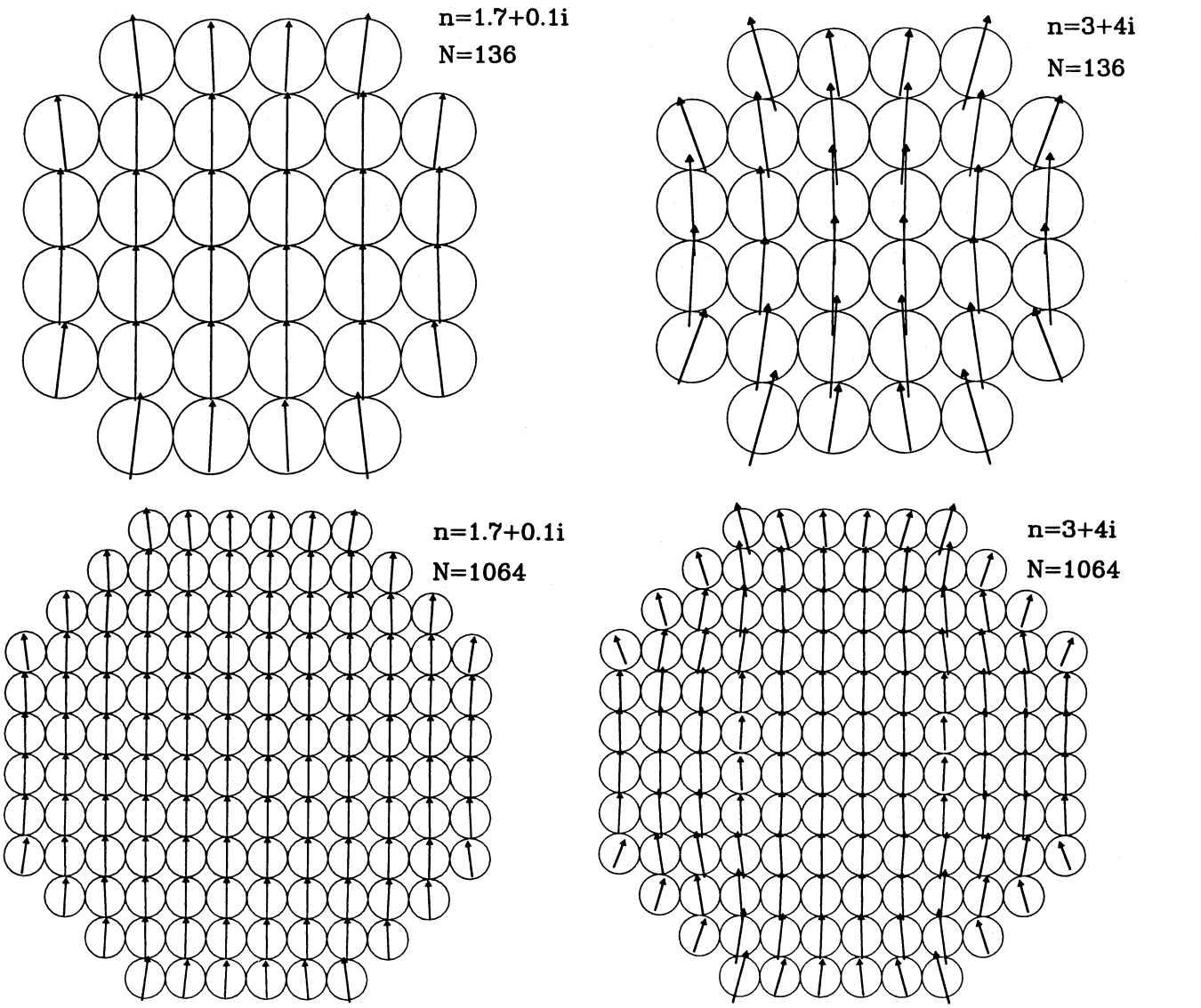

FIG. 2.—Dipole polarizations within "spheres" consisting of $N = 136$ and $N = 1064$ dipoles, in a static uniform applied electric field. The applied electric field is in the y-direction; shown are the dipoles lying on the $z = d/2$ plane. The four cases are labeled by the number N of dipoles and the complex refractive index n. The individual polarization vectors would be parallel and of length equal to d if the polarization per dipole were equal to the polarization within a continuum sphere (see text). It is seen that significant departures from the continuum limit occur at "corners" along the sphere boundary; the fraction of the array elements located along the boundary decreases as $N^{-1/3}$. It is also seen that departures from the continuum limit are more pronounced for large values of the refractive index m. As discussed in the text, this surface "granularity" is a significant source of error for large values of the refractive index m; suppression of this error may require very large values of N.

(3.05). To estimate the relative importance of magnetic dipole absorption, consider a spherical volume, of radius $r = (3/4\pi)^{1/3}d$, having the same volume as our unit cell. For this sphere the ratio of magnetic dipole absorption to electric dipole absorption is (Draine and Lee 1984)

$$\frac{C_{\rm abs}^m}{C_{\rm abs}^e} \approx \frac{(kr)^2}{90}\left[(\epsilon_1+2)^2+\epsilon_2^2\right]. \quad (4.03)$$

If we require $C_{\rm abs}^m/C_{\rm abs}^e < \Delta$, one obtains the condition $N \gtrsim (ka_{\rm eq})^3|m|^6\Delta^{-3/2}/90$ [where we have replaced $(\epsilon_1+2)^2+\epsilon_2^2$ by $|m|^4$, since magnetic dipole effects are important only for $|\epsilon| \gg 1$]; this can be combined with equation (4.02) to obtain a second validity criterion:

$$N \gtrsim \frac{4\pi}{3}(ka_{\rm eq})^3|m|^3\left(\frac{\Delta}{0.1}\right)^{-3}\left[1+\frac{|m|^3}{36\pi}\left(\frac{\Delta}{0.1}\right)^{3/2}\right]. \quad (4.04)$$

Evidently magnetic dipole effects are an important consideration when $|m| \gtrsim (36\pi)^{1/3}(\Delta/0.1)^{-1/2} = 4.83(\Delta/0.1)^{-1/2}$. For given N, the validity criterion (4.04) is equivalent to a limit on $ka_{\rm eq}$:

$$ka_{\rm eq} \lesssim (ka)_{\rm crit} \equiv \left(\frac{3N}{4\pi}\right)^{1/3}|m|^{-1}\left(\frac{\Delta}{0.1}\right) \times\left[1+\frac{|m|^3}{36\pi}\left(\frac{\Delta}{0.1}\right)^{3/2}\right]^{-1/3}. \quad (4.05)$$

V. METHOD OF SOLUTION

Solution of the equation $\tilde{\mathbf{A}}\tilde{\mathbf{P}} = \tilde{\mathbf{E}}_{\rm inc}$ by direct inversion of the matrix $\tilde{\mathbf{A}}$ is feasible only for small values of N, since the amount of computing required to effect matrix inversion scales as N^3 (see, e.g., Press *et al.* 1985). The storage requirements

may also be prohibitive if the entire ($3N \times 3N$) matrix $\mathbf{A}$ must be resident, since $144N^2$ bytes of storage are required if "double precision" numbers are used (16 bytes per complex number). If fourfold symmetry is exploited, so that the equation to be solved is $\tilde{\mathbf{B}}\tilde{P}' = \tilde{E}'_{\rm inc}$, the amount of storage is reduced to $9N^2$ bytes, but still amounts to 10 Megabytes for the $N = 1064$ grain models we consider here.

Purcell and Pennypacker (1973) used an iterative method which involved calculating the polarizations using the polarizations from the previous iteration to estimate the electric field at each dipole; they remarked that convergence was often slow and the method was sometimes unstable and nonconvergent.

Yung (1978) used an iterative scheme which appears to converge provided the imaginary component of the refractive index is small. Unfortunately, however, the algorithm described by Yung does not work for arbitrary complex matrices $\mathbf{A}$.

Singham and Bohren (1987) have pointed out that the polarization vectors $\boldsymbol{P}_j$ can be expanded in powers of the polarizabilities α_j. By iteratively substituting equation (2.04) for $\boldsymbol{P}_j$ in place of $\boldsymbol{P}_k$ appearing on the right-hand side of equation (2.04), one obtains (to fourth order in the α_j):

$$\boldsymbol{P}_j = \alpha_j \boldsymbol{E}_{\mathrm{inc},j} - \alpha_j \sum_{k\neq j} \mathbf{A}_{jk}\alpha_k \boldsymbol{E}_{\mathrm{inc},k} + \alpha_j \sum_{k\neq j} \mathbf{A}_{jk}\alpha_k \sum_{l\neq k} \mathbf{A}_{kl}\alpha_l \boldsymbol{E}_{\mathrm{inc},l} - \alpha_j \sum_{k\neq j} \mathbf{A}_{jk}\alpha_k \sum_{l\neq k} \mathbf{A}_{kl}\alpha_l \sum_{m\neq l} \mathbf{A}_{lm}\alpha_m \boldsymbol{E}_{\mathrm{inc},m} + O(\alpha^5) . \quad (5.01)$$

For sufficiently small α_j and sufficiently small values of kd, this expansion is rapidly convergent, and it therefore provides an excellent method to obtain the $\boldsymbol{P}_j$ in the limit $|\epsilon - 1| \lesssim 1$. To obtain the M independent elements of the $\boldsymbol{P}_j$ to nth order in α requires $(n-1)M^2$ complex scalar multiplications ($M = 3N$ for the general scattering problem, or $M = 3N/4$ if fourfold symmetry is exploited). Since equation (5.01) is not generally convergent, however, we still require a procedure which is sufficiently robust to solve the general scattering problem.

Petravic and Kuo-Petravic (1979) have described a general class of conjugate gradient algorithms. The calculations reported here have used the special case of this algorithm which occurs when the arbitrary positive Hermitian matrices $\mathbf{H}$ and $\mathbf{K}$ in their method are each simply taken to be the identity matrix. The resulting iteration scheme is as follows: to solve a system $Cx = y$, start with an initial guess x_0 and set

$$z \equiv C^\dagger y , \quad (5.02)$$

$$g_0 = z - C^\dagger C x_0 , \quad (5.03)$$

$$p_0 = g_0 , \quad (5.04)$$

$$w_0 = C x_0 , \quad (5.05)$$

$$v_0 = C p_0 , \quad (5.06)$$

and iteratively improve the estimate x_i using the recursion relations, beginning with $i = 0$:

$$\alpha_i = \frac{\langle g_i | g_i \rangle}{\langle v_i | v_i \rangle} , \quad (5.07)$$

$$x_{i+1} = x_i + \alpha_i p_i , \quad (5.08)$$

$$w_{i+1} = w_i + \alpha_i v_i , \quad (5.09)$$

$$g_{i+1} = z - C^\dagger w_{i+1} , \quad (5.10)$$

$$\beta_i = \frac{\langle g_{i+1} | g_{i+1} \rangle}{\langle g_i | g_i \rangle} , \quad (5.11)$$

$$p_{i+1} = g_{i+1} + \beta_i p_i , \quad (5.12)$$

$$v_{i+1} = C g_{i+1} + \beta_i v_i . \quad (5.13)$$

In the above equations $C^\dagger$ is the Hermitian conjugate of C: $(C^\dagger)_{jk} = (C_{kj})^*$. The computational burden in this numerical scheme consists primarily of evaluation of equations (5.10) and (5.13), each of which requires multiplication of a vector by a matrix. If the vector has dimension M, each such matrix-vector multiplication involves M^2 complex scalar multiplications. Therefore, in the limit of large M the scheme requires $\sim 2M^2$ (complex) scalar multiplications per iteration. For a nonzero initial guess x_0 there is also a "startup" cost of $4M^2$ complex scalar multiplications (to evaluate Cx_0, $C^\dagger C x_0$, $C^\dagger y$, and Cp_0); if $x_0 = 0$ is taken for the initial guess, the startup cost is reduced to $2M^2$ complex scalar multiplications. This is the minimum computational overhead; if memory limitations do not permit storage of the matrix C, then additional computations will be required to evaluate the elements of C as they are needed in the course of performing the matrix-vector multiplications ($2M^2$ evaluations per iteration).

In the above iteration scheme, the vectors v_i and w_i are actually defined by the defining relations

$$v_i \equiv C p_i , \quad (5.14)$$

$$w_i \equiv C x_i . \quad (5.15)$$

To minimize computing, the iteration scheme does not compute new values v_{i+1} and w_{i+1} from equations (5.14) and (5.15), which would require two matrix-vector multiplications, but instead through equations (5.09) and (5.13), using only a single matrix-vector multiplication. Because of roundoff error, however, the computed value of v_i and w_i may deviate from equations (5.14) and (5.15). Every 10 iterations, then, v_i and w_i are recomputed using the defining relations (5.14) and (5.15).

The numerical implementation developed by the author takes advantage of the fact that many of the elements of the basic 3×3 matrices $\mathbf{A}_{jk}$ defined by equations (2.06) and (2.07)—which provide the "elements" of the $3N \times 3N$ symmetric matrix $\tilde{A}$, or the $(3N/4) \times (3N/4)$ symmetric matrix $\tilde{B}$ if fourfold symmetry is being exploited—depend only on the displacement $\boldsymbol{r}_{jk}$ between dipole locations j and k. Since the dipoles are assumed to be located on a simple cubic lattice, it follows that many different (j, k) pairs of dipoles have common values of $\boldsymbol{r}_{jk}$ and hence $\mathbf{A}_{jk}$. For N lattice sites within a convex region of volume Nd^3, the number of distinct $\boldsymbol{r}_{jk}$ vectors is $\lesssim 4N$; thus it suffices to compute and store only $\sim 4N$ 3×3 matrices A_{jk}. Since the matrices A_{jk} are themselves symmetric, and the diagonal elements are trivial, it suffices to store only three independent elements per matrix; thus this approach requires storage of $\lesssim 12N$ complex numbers, small compared to the $9N^2$ complex numbers which comprise the full matrix $\tilde{\mathbf{A}}$ (or $9N^2/16$ complex numbers for $\tilde{\mathbf{B}}$). Of course, this economy of storage is purchased at the price of the computational overhead needed to identify which of the stored numbers corresponds to the desired element of $\tilde{\mathbf{A}}$.

The FORTRAN program used in the calculations reported below, in which fourfold symmetry is exploited, occupies ~ 1 Megabyte of memory, sufficient to handle grains with $N \lesssim$

TABLE 1

NUMBER OF ITERATIONS REQUIRED FOR CONVERGENCE[a] USING $x_0 = 0$ AS STARTING POINT

m	ka_{eq}	$N = 136$	$N = 304$	$N = 1064$	$N = 2320$
1.33	0.1	2	...	2	...
	0.5	2	2	2	...
	1	2	2	2	...
	2	4	4	4	...
	5	9	9	10	...
$1.7 + 0.1i$	0.1	3	3	3	3
	0.5	4	4	4	4
	1	4	5	4	4
	2	6	6	6	7
	5	24	23	12	14
$3 + 4i$	0.1	28	33	39	40
	0.5	30	37	38	42
	1	12	42	41	41
	2	25	33	19	16

[a] Convergence is considered to have been attained when Q_{ext} is within 1% of the fully converged discrete-dipole solution, and remains within 1% on all subsequent iterations.

2500. On a Vax 780 or Vax 8200, one iteration requires $\sim 400(N/1000)^2$ cpu sec.

The number of iterations required to obtain an accurate solution depends upon the grain shape, N, the refractive index, ka_{eq}, and the initial starting point x_0. Tables 1 and 2 show the number of conjugate-gradient iterations required for convergence for calculations of scattering by spheres with $N = 136$, 304, 1064, and 2320 for two refractive indices, and several different values of ka_{eq}; Table 1 shows the number of iterations required starting from an initial guess $x_0 = 0$, while Table 2 shows the number of iterations required when the fourth-order expansion equation (5.01) is used to generate x_0. For Tables 1 and 2 a solution is considered to be "converged" if all subsequent iterations give Q_{ext} within 1% of the exact Q_{ext} for the dipole array being considered;[5] in practice, additional iterations are required to demonstrate that convergence has been attained, but the numbers in Tables 1 and 2 are useful for showing how the speed of convergence varies from one scattering problem to another. There is clearly a tendency for convergence to be slower for the larger refractive index. To some extent there is also a tendency for more iterations to be required for larger values of ka_{eq}, and for larger N values, but exceptions to these trends are apparent. It is also seen that the fourth-order expansion (eq. [5.01]) can be used to obtain good solutions (requiring few, if any, subsequent iterations) for small values of $|m - 1|$, but the conjugate gradient method also converges rapidly for such cases. Recall that the expansion (5.01) requires $\sim 3M^2$ multiplications to evaluate x_0, plus another $\sim 4M^2$ multiplications in "startup" cost for the iteration procedure, for a total of $7M^2$ complex multiplications; use of $x_0 = 0$, on the other hand, requires only $2M^2$ multiplications before the iterative procedure begins. Thus use of the expansion (5.01) "costs" an additional $5M^2$ multiplications, comparable to the cost of 2–3 additional iterations (assuming $2M^2$ multiplications per iteration). While a valuable aid, the expansion (5.01) therefore leads to only a modest reduction in computational requirements even within its domain of convergence; for large values of $|m - 1|$ or ka_{eq} (e.g., $m = 1.33$, $ka_{eq} = 5$, or $m = 3 + 4i$, $ka_{eq} = 2$) taking $x_0 = 0$ for the initial guess is actually preferable to using equation (5.01).

[5] The "exact" solution to the discrete dipole scattering problem is obtained by iterating with the conjugate gradient method until the equation $\tilde{\mathbf{A}}\tilde{P} = \tilde{E}_{inc}$ (or $\tilde{\mathbf{B}}\tilde{P}' = \tilde{E}'_{inc}$) is satisfied to high accuracy.

TABLE 2

NUMBER OF ITERATIONS REQUIRED FOR CONVERGENCE[a] USING x_0 FROM FOURTH-ORDER EXPANSION

m	ka_{eq}	$N = 136$	$N = 1064$
1.33	0.1	0	0
	0.5	0	0
	1	0	0
	2	2	2
	5	10	10
$3 + 4i$	0.1	21	27
	0.5	20	32
	1	19	18
	2	40	...

[a] Convergence is considered to have been attained when Q_{ext} is within 1% of the fully converged discrete-dipole solution, and remains within 1% on all subsequent iterations.

VI. ACCURACY: COMPARISON WITH MIE THEORY FOR SPHERES

To test the accuracy of the discrete dipole method, Purcell and Pennypacker (1973) and Yung (1978) have carried out computations for discrete dipole models of homogeneous, isotropic spheres, for which Mie scattering theory provides exact solutions. Additional such calculations are reported here.

Purcell and Pennypacker (1973) showed results for $N = 136$ and two cases: $m \equiv \epsilon^{1/2} = 1.33$ and $m = 1.7 + 0.1i$. Additional results are reported here for the case $m = 1.7 + 0.1i$, for which equation (4.02) gives $N_{min} \approx 21(\Delta/0.1)^{-3}$. Figure 3*a* shows results for $Q_{ext} \equiv C_{ext}/\pi a^2$ and $Q_{abs} \equiv C_{abs}/\pi a^2$ for discrete-dipole models of spheres with $N = 136$, $N = 304$, and $N = 1064$, together with Mie theory results (*solid lines*). Figures 3*b* and 3*c* show results for the albedo and scattering asymmetry parameter $g = \langle \cos\theta \rangle$. It is seen that agreement is excellent for small values of $x = 2\pi a_{eq}/\lambda$. According to the validity criterion (4.05) (taking $\Delta = 0.1$), one would expect the discrete dipole models to be accurate (to within $\sim 10\%$) for $ka_{eq} \lesssim (ka)_{crit} = 3.70(N/1064)^{1/3}$. In Figure 3*d* we show the fractional error in the computed extinction as a function of $ka_{eq}/(ka)_{crit}$. It is indeed seen that appreciable errors begin to appear when $ka_{eq}/(ka)_{crit} \gtrsim 1$, just as expected.

The above results confirm the ability of the discrete dipole model to satisfactorily model grains whose refractive index has at most a small imaginary component: neither Purcell and Pennypacker (1973) nor Yung (1978) considered grains with a refractive index having a large imaginary component. Figures 4*a*–4*d* shows the results of calculations carried out for $m = 3 + 4i$ ($\epsilon = -7 + 24i$). For $m = 3 + 4i$ equation (4.01) gives $N_{min} = 670(\Delta/0.2)^{-3}$, so that we may expect to achieve $\sim 20\%$ accuracy in the zero-frequency limit for $N = 1064$. As discussed in § IV*a*, the granularity of the surface leads to appreciable errors even in the zero-frequency limit; this overestimate of Q_{abs} and Q_{ext} tends to persist even when the wavelength becomes comparable to the grain radius, as seen in Figure 4*a*. In Figure 4*b* we see that the overestimation of Q_{abs} due to surface granularity leads to underestimation of the albedo. The scattering asymmetry parameter in Figure 4*c* follows the expected trend, although with a tendency toward excessive forward scattering. In Figure 4*d* we show the fractional error in the extinction cross section as a function of $ka_{eq}/(ka)_{crit}$, where $(ka)_{crit} = 0.99(N/1064)^{1/3}$ is again obtained

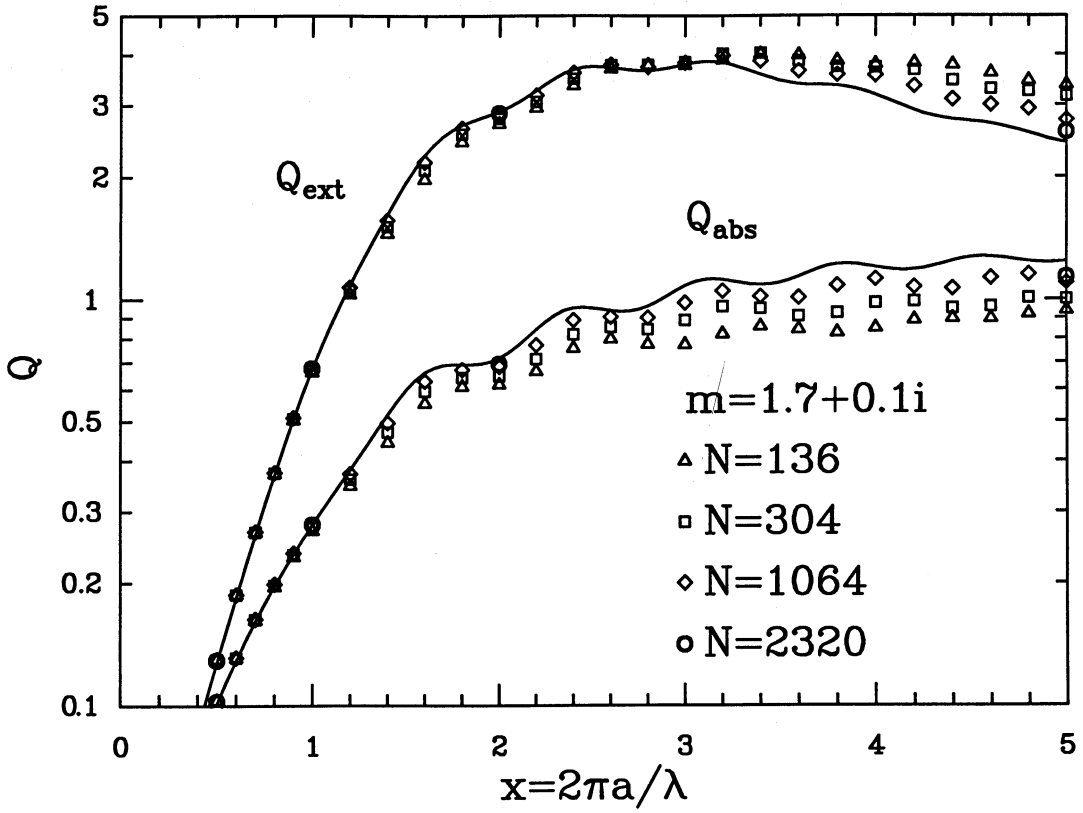

FIG. 3*a*

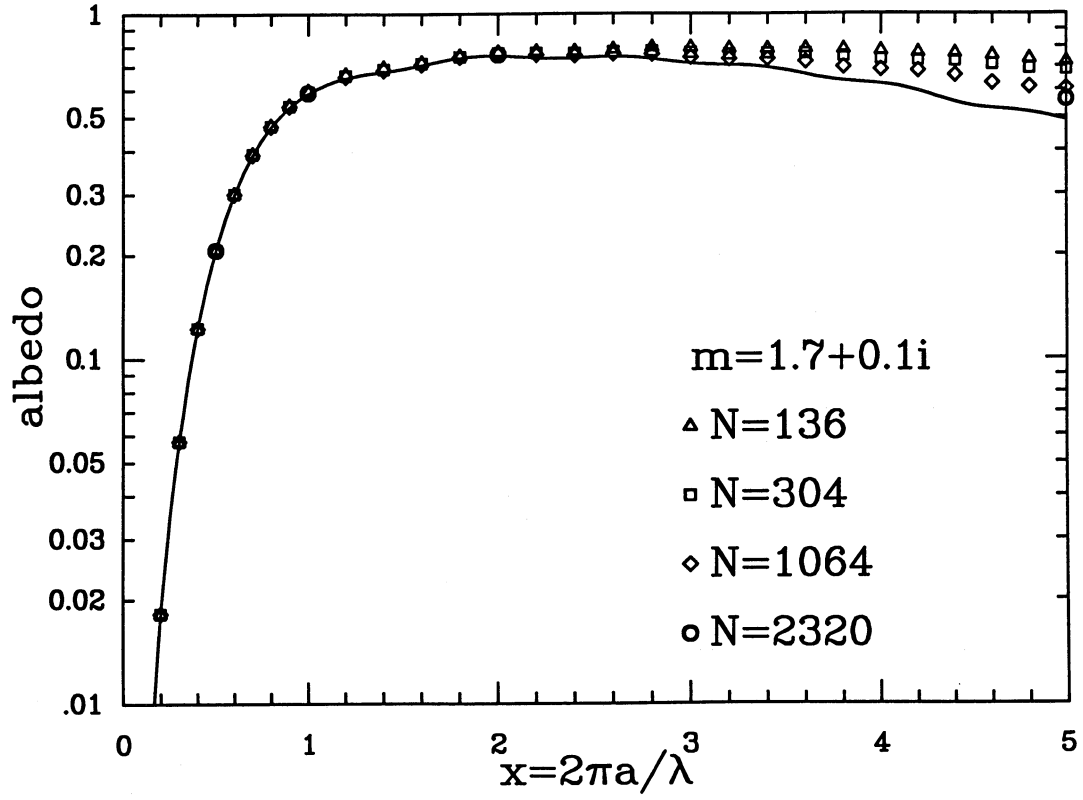

FIG. 3*b*

FIG. 3.—(*a*) Extinction and absorption efficiency factors for "spheres" with refractive index $m = 1.7 + 0.1i$, as a function of $x = 2\pi a/\lambda$, where a is the "equivalent" radius of a sphere having equal volume. Solid curve is the exact result for a true sphere ($N \to \infty$), obtained using Mie theory. Results are shown for $N = 136$, 304, and 1064. (*b*) Same as (*a*), but showing the albedo $\equiv Q_{sca}/Q_{ext}$. (*c*) Same as (*a*), but showing the scattering asymmetry factor $g \equiv \langle \cos\theta \rangle$. (*d*) Fractional "error" in the extinction cross section, as a function of $ka/(ka)_{crit}$, for $n = 1.7 + 0.1i$ and three different values of N.

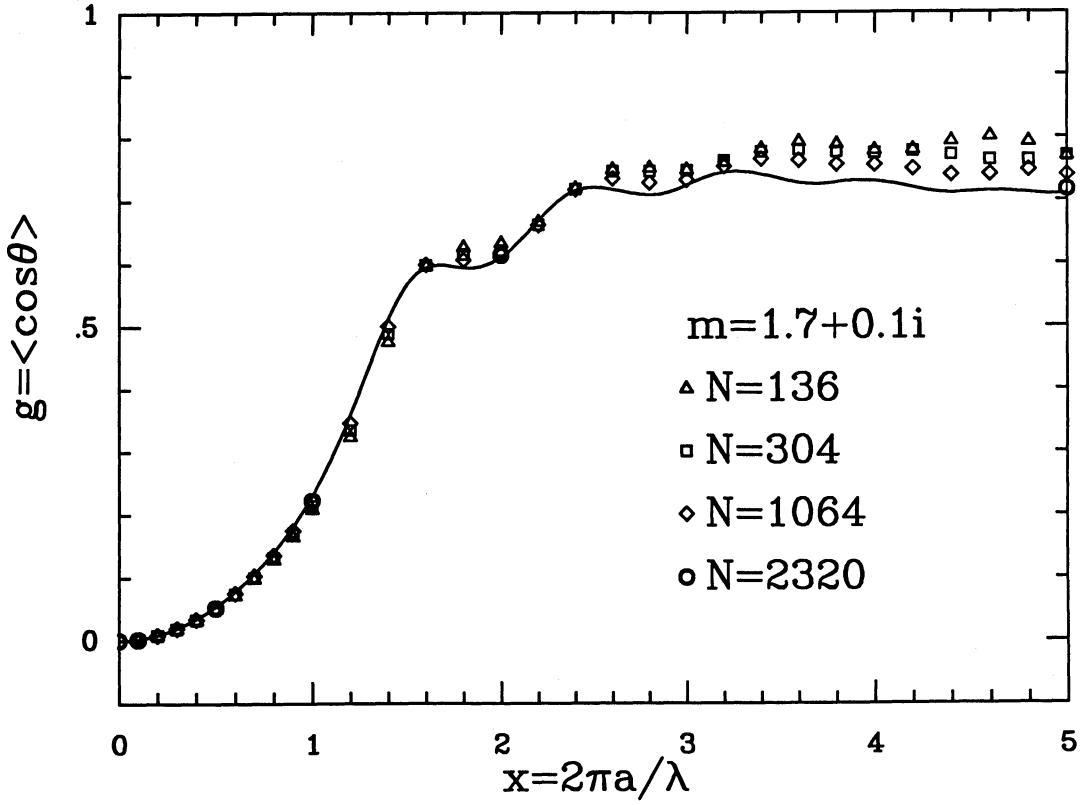

FIG. 3*c*

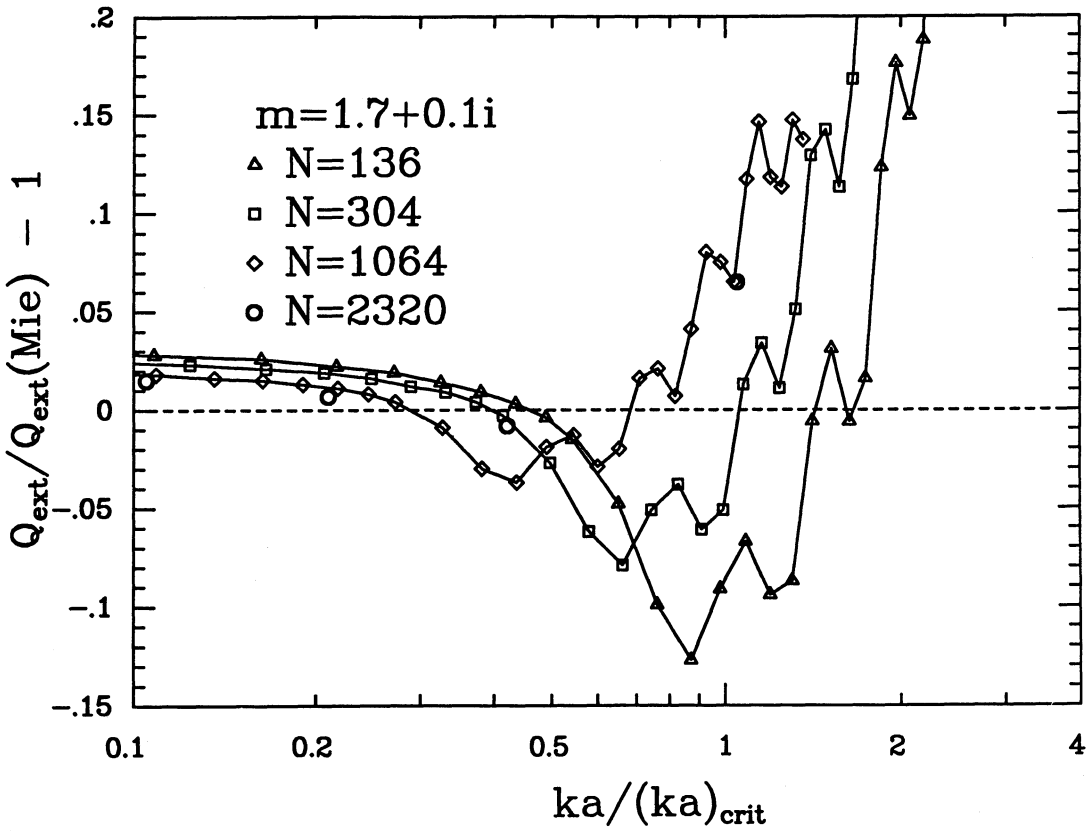

FIG. 3*d*

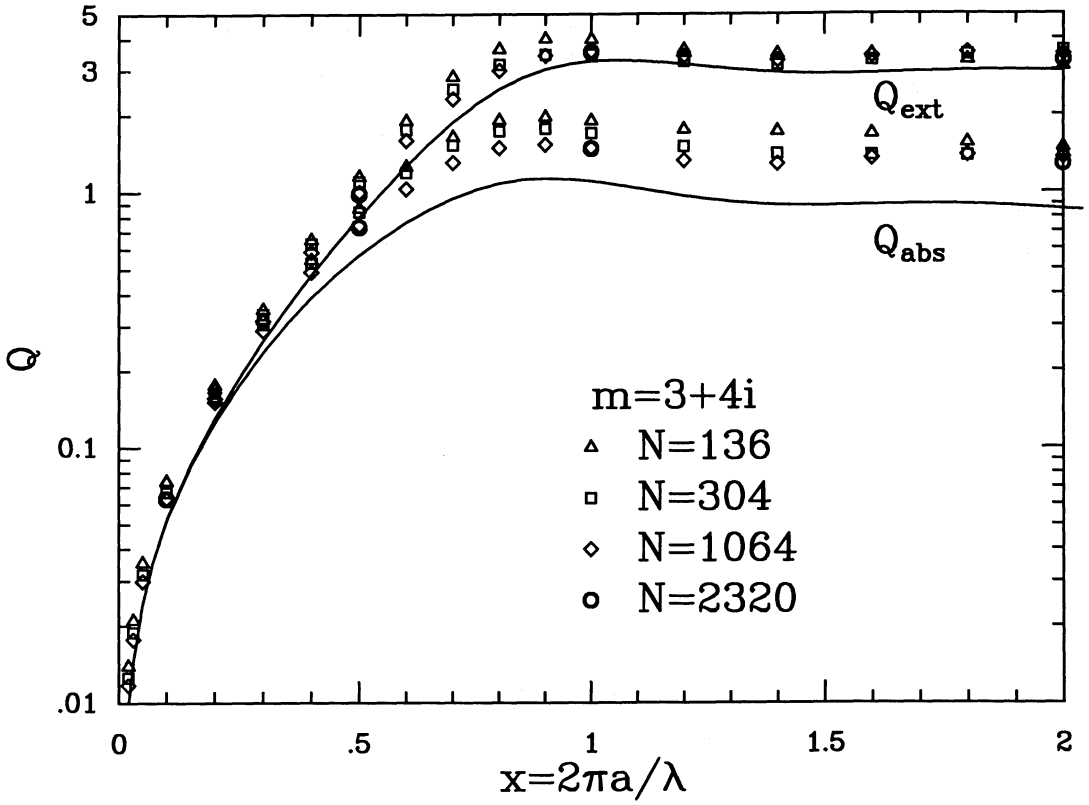

FIG. 4*a*

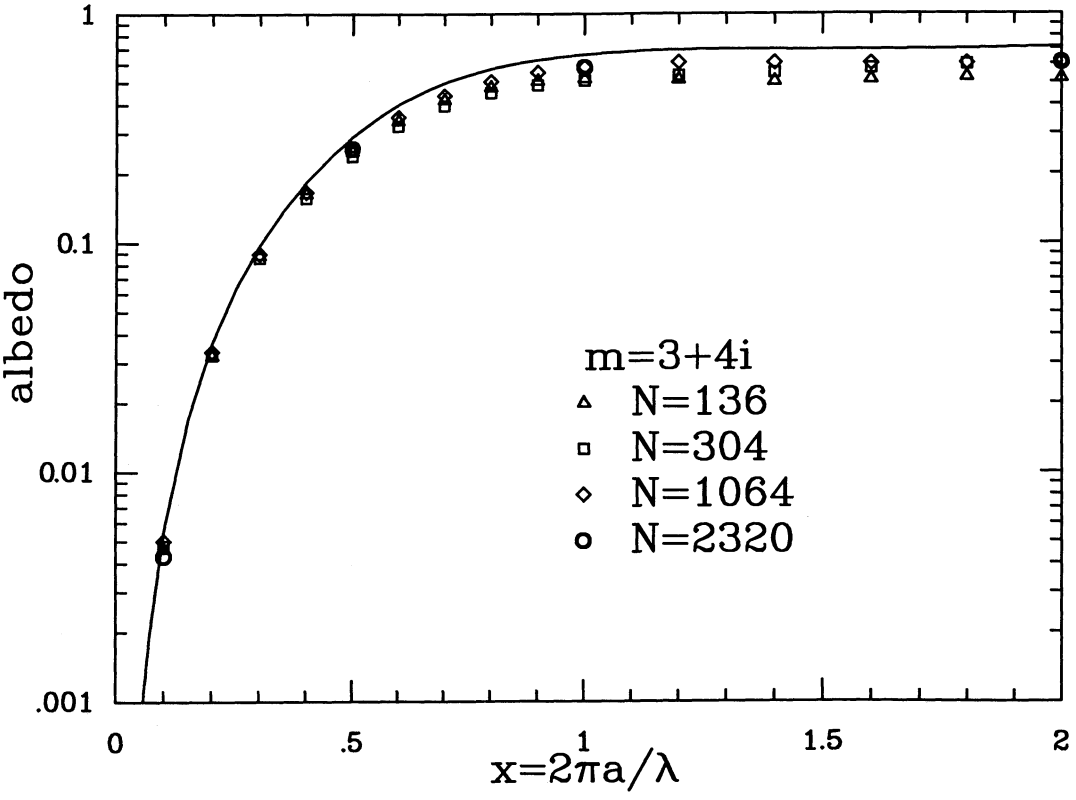

FIG. 4*b*

4.—(*a*)–(*d*) Same as Fig. 3, except for $m = 3 + 4i$. In (*d*) it is seen that the fractional error is appreciable even in the zero-frequency limit, as a result of "surface
arity."

FIG.
granula

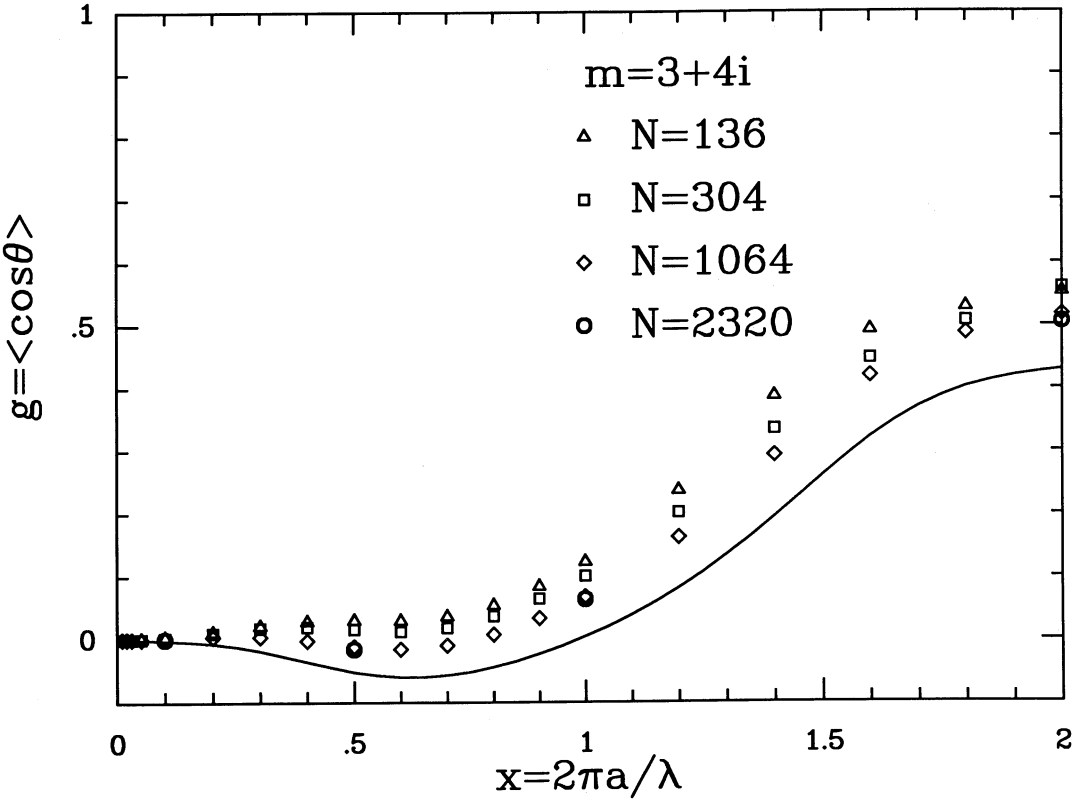

FIG. 4c

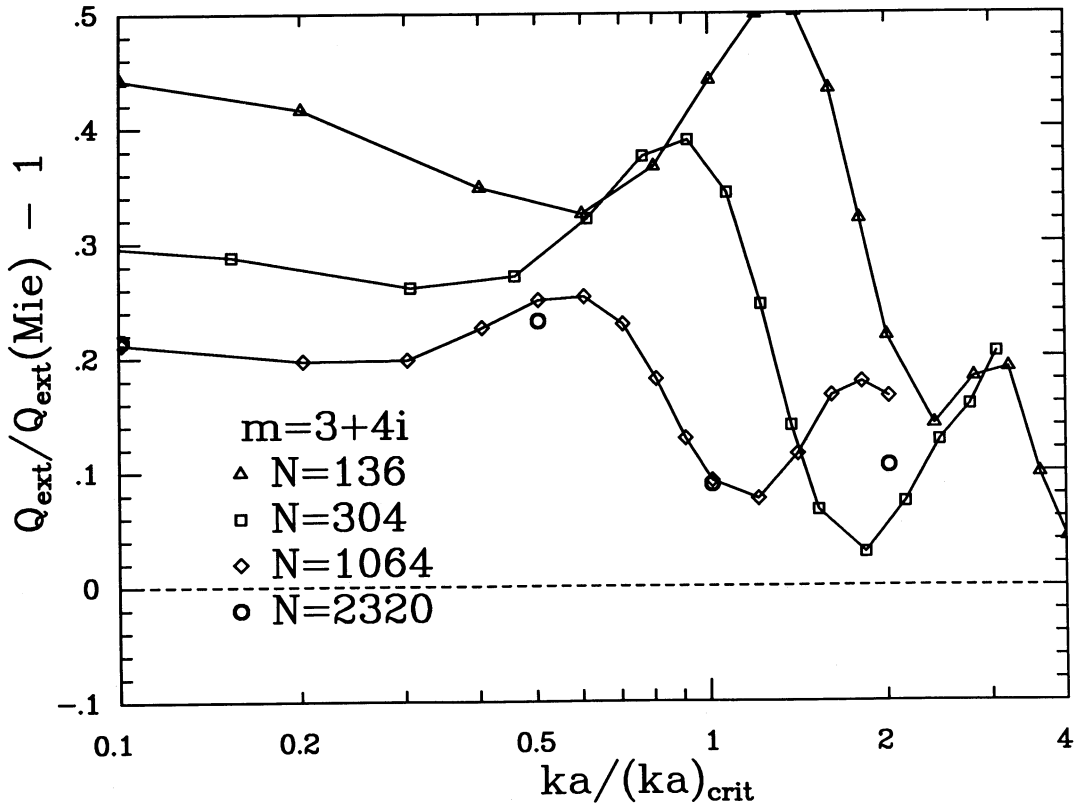

FIG. 4d

from equation (4.05) with $\Delta = 0.1$. For small values of $ka_{eq}/(ka)_{crit}$, the (substantial) errors are due to the surface granularity of the grains; additional error (sometimes of opposite sign) is present for $ka_{eq} \gtrsim (ka)_{crit}$.

Based upon the above comparisons with Mie theory, we conclude that the discrete dipole model appears to be valid, provided the validity criteria (4.01) and (4.05) are satisfied.

VII. GRAPHITE SPHERES

The observed interstellar extinction includes a prominent feature at 2175 Å (the reader is referred to the detailed observational studies by Savage 1975; Carnochan 1986; Fitzpatrick and Massa 1986). Although a variety of explanations for this feature have been proposed, identification of the grain material responsible for the feature remains uncertain. Graphite, however, has been frequently considered because small graphite spheres are expected to display an extinction peak at approximately the correct wavelength; the extinction peak is due to a "plasma resonance" which, for small spheres, occurs when Re $(\epsilon_\perp) = -2$ (see Gilra 1972). Carbon is a sufficiently abundant element that attribution of the 2175 Å feature to graphite does not conflict with cosmic abundance constraints.

Theoretical computation of absorption and scattering by graphite particles is considerably complicated by the fact that graphite is a highly anisotropic material. The carbon atoms in graphite are organized into planar sheets; the so-called "c-axis" of the graphite crystal is normal to the graphite plane. The response of graphite to an electric field differs greatly depending on whether the field is normal to the plane ($\boldsymbol{E} \parallel c$) or parallel to the plane ($\boldsymbol{E} \perp c$). In a coordinate system with the x-axis parallel to the c-axis, the graphite dielectric tensor is diagonal, with diagonal elements $(\epsilon_\parallel, \epsilon_\perp, \epsilon_\perp)$. Even for the simplest possible shape—a sphere—there is no analytic theory for the scattering and absorption of light when the material of which the sphere is composed is anisotropic, except in the "electric dipole limit" when the sphere is very small compared to the wavelength. Therefore, calculations of the absorption and scattering of light by interstellar graphite spheres have generally resorted to what may be termed the "$\frac{1}{3}$–$\frac{2}{3}$ approximation": one replaces an ensemble of (randomly oriented) graphite spheres by a mixture of two different hypothetical particles—$\frac{1}{3}$ of the particles consist of a hypothetical isotropic material with $\epsilon = \epsilon_\parallel$, and $\frac{2}{3}$ of the particles consist of an isotropic material with $\epsilon = \epsilon_\perp$. While this "$\frac{1}{3}$–$\frac{2}{3}$ approximation" is in fact exact in the "electric dipole" limit ($a/\lambda \to 0$), it has no particular justification (other than expediency) when the particle size becomes comparable to the wavelength. Nevertheless, the approximation has been widely employed, for lack of a better estimator of the scattering and absorption cross sections of graphite spheres. The accuracy of the approximation has apparently not hitherto been examined.

In this section we will examine the validity of the "$\frac{1}{3}$–$\frac{2}{3}$" approximation, by computing scattering and extinction cross sections for anisotropic graphite spheres using the discrete dipole method, and then comparing these results with estimates obtained using the "$\frac{1}{3}$–$\frac{2}{3}$" approximation and Mie theory. Since interest in graphite has been mainly stimulated by the 2175 Å extinction feature, we will restrict our attention to the ultraviolet ($\lambda < 3300$ Å). The wavelength-dependent dielectric tensor is taken from Draine and Lee (1984; see also Draine 1985), and is based on laboratory measurements on bulk graphite. It should be applicable to particles with $a_{eq} \gtrsim 100$ Å, for which $\lesssim 6\%$ of the carbon atoms are in the surface monolayer. Over the range 3000–1000 Å, both $\epsilon_\perp$ and $\epsilon_\parallel$ vary appreciably; the largest values of $|m-1|$ occur at 2800 Å ($m_\perp = 2.11 + 2.3i$, $|m_\perp - 1| = 2.58$) and 1100 Å ($m_\parallel = 1.73 + 2.14i$, $|m_\parallel - 1| = 2.28$).

Before actually addressing real anisotropic graphite, we test our discrete dipole calculation on hypothetical isotropic spheres with $\epsilon = \epsilon_\perp$, where we can compare our results with Mie theory. Over the wavelength range $3 < \lambda^{-1} < 7\ \mu\text{m}^{-1}$, the validity criterion (4.05) (taking $\Delta = 0.1$) is most stringent at $\lambda^{-1} = 3.6\ \mu\text{m}^{-1}$, where it translates into the condition $a_{eq} \lesssim 735(N/1064)^{1/3}$ Å.

In Figure 5*a*, we show Q_{ext} for such a sphere with $a = 100$ Å; the squares show the results of discrete dipole calculations with $N = 1064$, while the solid curve is Mie theory for an exact sphere. We see that granularity of the discrete dipole model introduces systematic errors: the discrete dipole model overestimates Q_{ext} for $\lambda^{-1} < 4.6\ \mu\text{m}^{-1}$, and underestimates it for $\lambda^{-1} > 4.6\ \mu\text{m}^{-1}$; similar errors are seen for $a = 200$ Å grains in Figure 5*b*. However, in no case is the error greater than 15%, and usually it is much smaller (the rms deviations for the points shown in Figs. 5*a* and 5*b* are 6.8% and 5.8%, respectively). Based on this comparison, we conclude that the discrete dipole model with $N = 1064$ can be used to estimate cross sections of $a_{eq} \lesssim 300$ Å graphite grains to within $\sim 10\%$.

Turning now to anisotropic graphite spheres, we show in Figures 6*a* and 7*a* the extinction cross section for randomly oriented graphite spheres, with radii $a = 100$ Å and $a = 200$ Å, respectively, computed using the $N = 1064$ discrete dipole model. The dotted lines in Figures 6*a* and 7*a* are computed using the "$\frac{1}{3}$–$\frac{2}{3}$" approximation, which evidently provides surprisingly good accuracy, at least for $a \lesssim 200$ Å! The broken lines in Figures 6*a* and 7*a* show two different estimates for the profile of the mean observed 2175 Å extinction feature (Fitzpatrick and Massa 1986); the narrower curve is a Drude fit to the feature, while the broader curve is the Drude fit plus 25% of the continuous extinction in the 3.3–5.9 μm^{-1} region.

In Figures 6*b* and 7*b* we show the linear and circular polarization efficiencies for two graphite spheres. It is assumed that the graphite spheres are aligned with $c \perp \boldsymbol{k}$, and $Q_{pol} \equiv [C_{ext}(c \perp \boldsymbol{E}) - C_{ext}(c \parallel \boldsymbol{E})]/\pi a^2$. The circular polarization efficiency factor is defined by $Q_{cpol} \equiv [C_{pha}(c \perp \boldsymbol{E}) - C_{pha}(c \parallel \boldsymbol{E})]/\pi a^2$.

It is interesting to note that the circular polarization cross section changes sign at a wavelength λ_c very close to the wavelength λ_{max} where the linear polarization cross section peaks (just as for the observed interstellar polarization at visual wavelengths). This can be understood on the basis of the Kramers-Kronig relations relating linear dichroism and birefringence, first pointed out by Shapiro (1975) (see also Martin 1975*a*, *b*). The Kramers-Kronig relations imply that if the linear polarization feature has the symmetry property $C_{pol}(\lambda) = C_{pol}(\lambda_{max}^2/\lambda)$, for arbitrary λ (at least within the range where the linear polarization cross section is appreciable), then it follows that $\lambda_{max} = \lambda_c$. It is interesting that the graphite polarization feature also has the property $\lambda_{max} \approx \lambda_c$, even though the graphite linear polarization does not have the above "symmetry."

VIII. NONSPHERICAL GRAPHITE PARTICLES

Because of the extreme anisotropy of its physical properties, graphite is not expected to form spherical particles. Because of the strong in-plane chemical bonds, and the relatively weak interplane attraction, small graphite crystallites of fixed mass

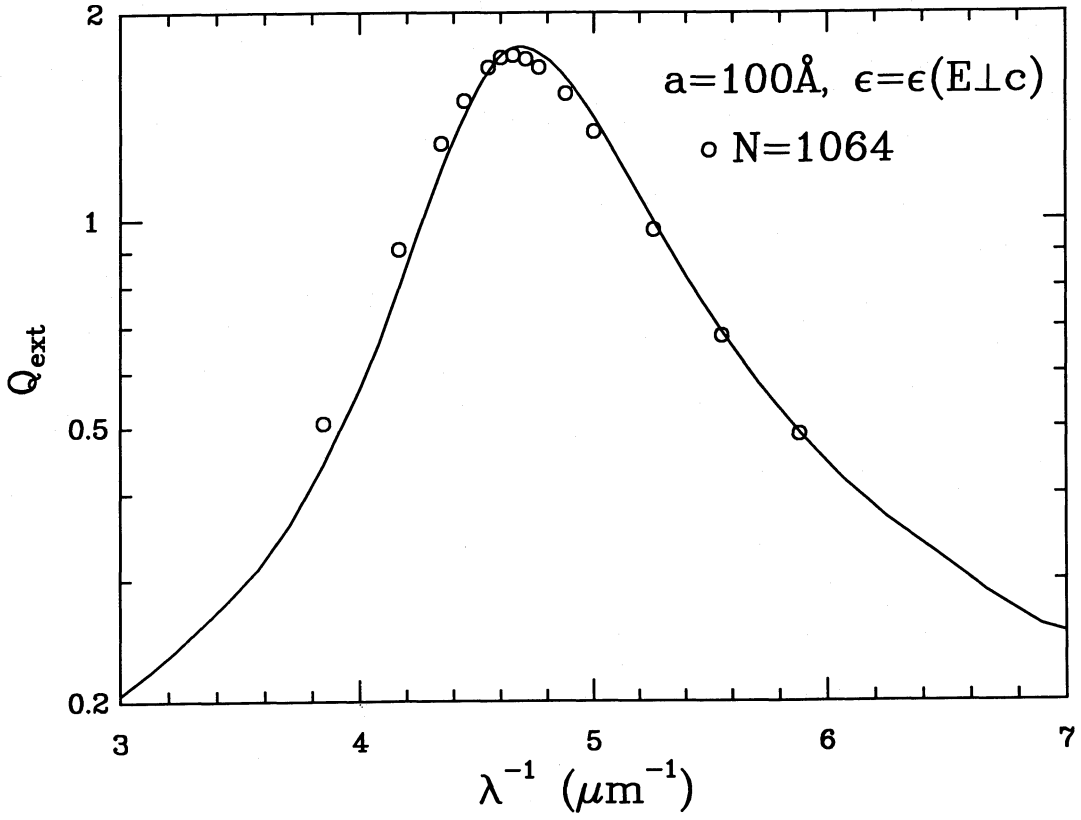

FIG. 5a

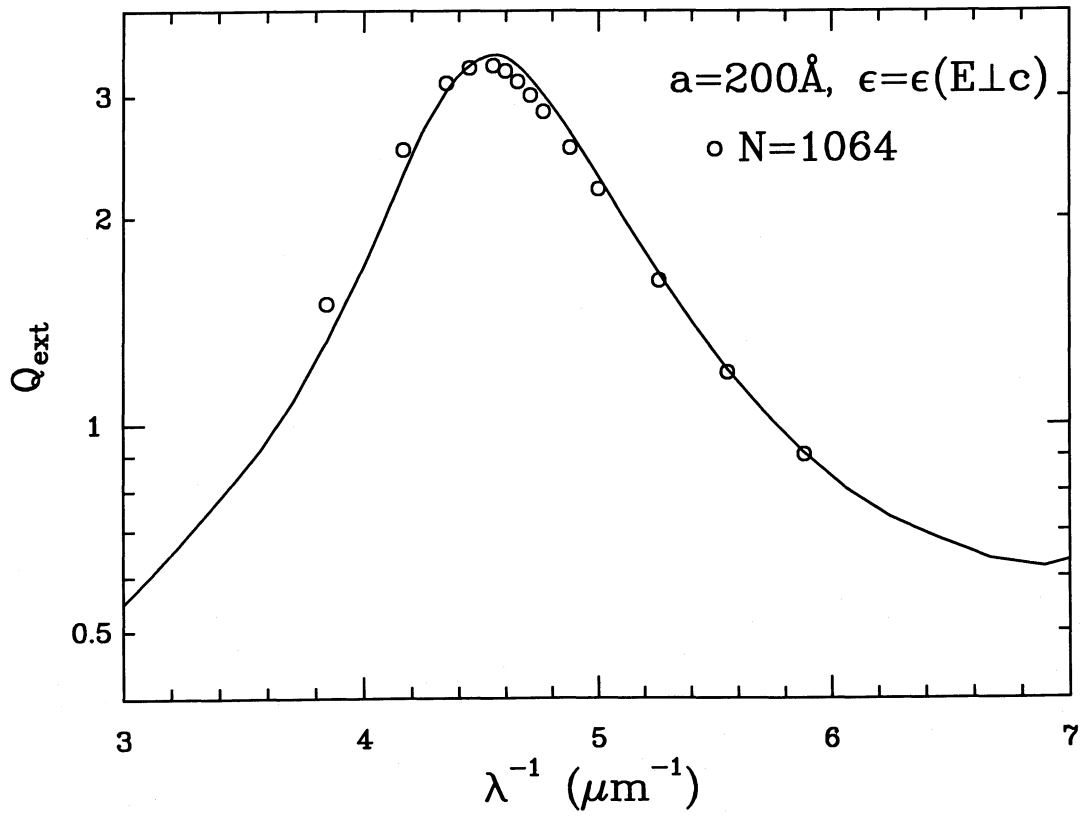

FIG. 5b

FIG. 5.—(*a*) Extinction cross section for a hypothetical sphere having a wavelength-dependent refractive index equal to that of the "$E \perp c$" component of graphite. Solid curve is the result for a perfect sphere with $a = 100$ Å, obtained from Mie theory; circles show results obtained for an $N = 1064$ discrete dipole array with $a_{eq} = 100$ Å. (*b*) Same as (*a*), but for $a = a_{eq} = 200$ Å.

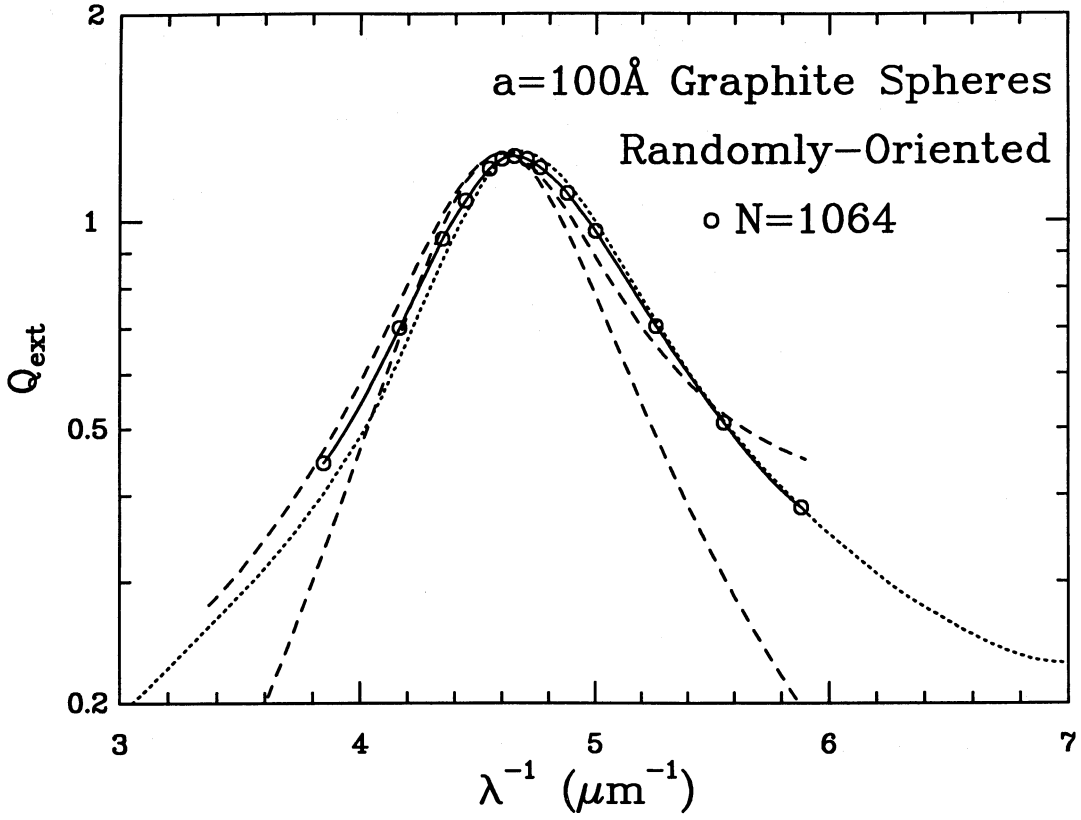

FIG. 6*a*

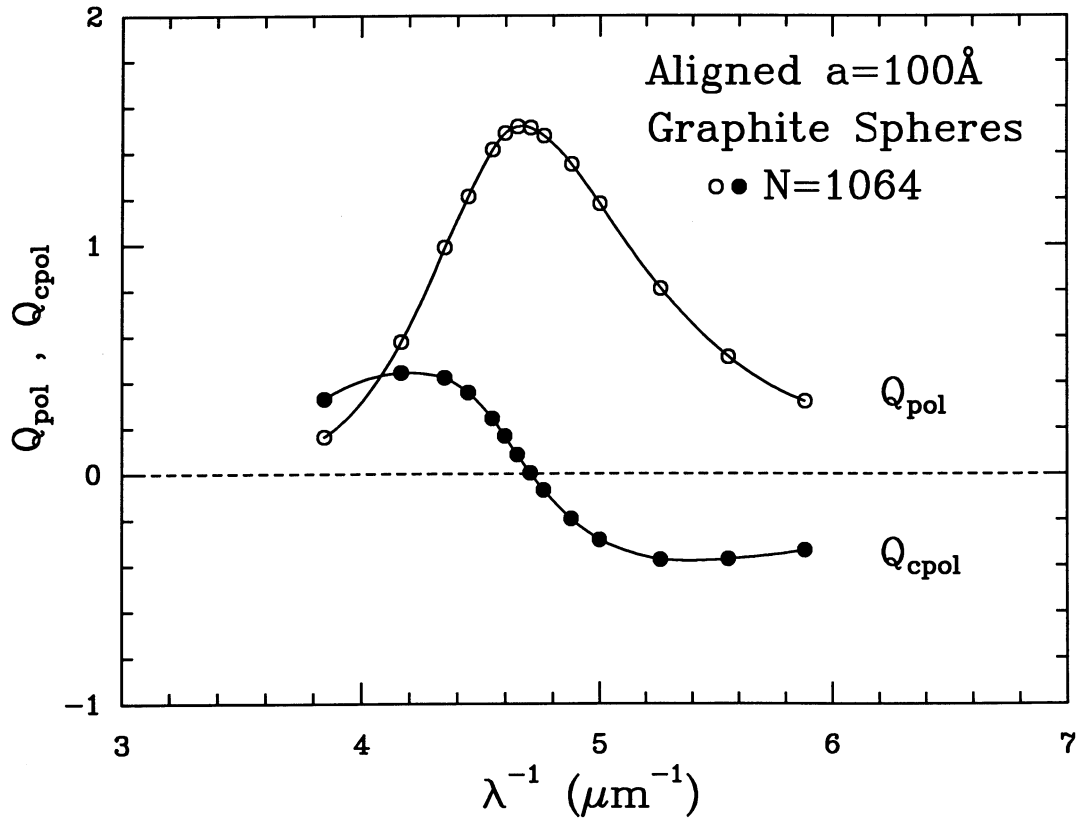

FIG. 6*b*

FIG. 6.—(*a*) Extinction efficiency factor for randomly oriented $a = 100$ Å spheres with the anisotropic refractive index of graphite. Circles show results of discrete dipole calculations for $N = 1064$ arrays with $a_{eq} = 100$ Å; dotted line shows the "$\frac{1}{3}$–$\frac{2}{3}$" approximation in which it is assumed that the ensemble of randomly-oriented graphite spheres can be replaced by a mixture of isotropic spheres, $\frac{1}{3}$ having $\epsilon = \epsilon_{||}$, and $\frac{2}{3}$ having $\epsilon = \epsilon_{\perp}$. The "$\frac{1}{3}$–$\frac{2}{3}$" approximation is seen to be surprisingly accurate for $a = 100$ Å. Also plotted (*broken curves*) are the estimates of Fitzpatrick and Massa (1986) for the 3.35–5.9 μm^{-1} extinction feature plus 0.0 and 0.25 of the mean continuum extinction; to facilitate comparison, these curves are plotted so their maxima attain a peak equal to the peak Q_{ext} value of the graphite particle. (*b*) Efficiency factors for linear and circular polarization (see text). Q_{pol} peaks at $\lambda^{-1}_{pol,max} \approx 4.67\ \mu m^{-1}$; Q_{cpol} changes sign at $\lambda_c^{-1} \approx 4.71\ \mu m^{-1}$.

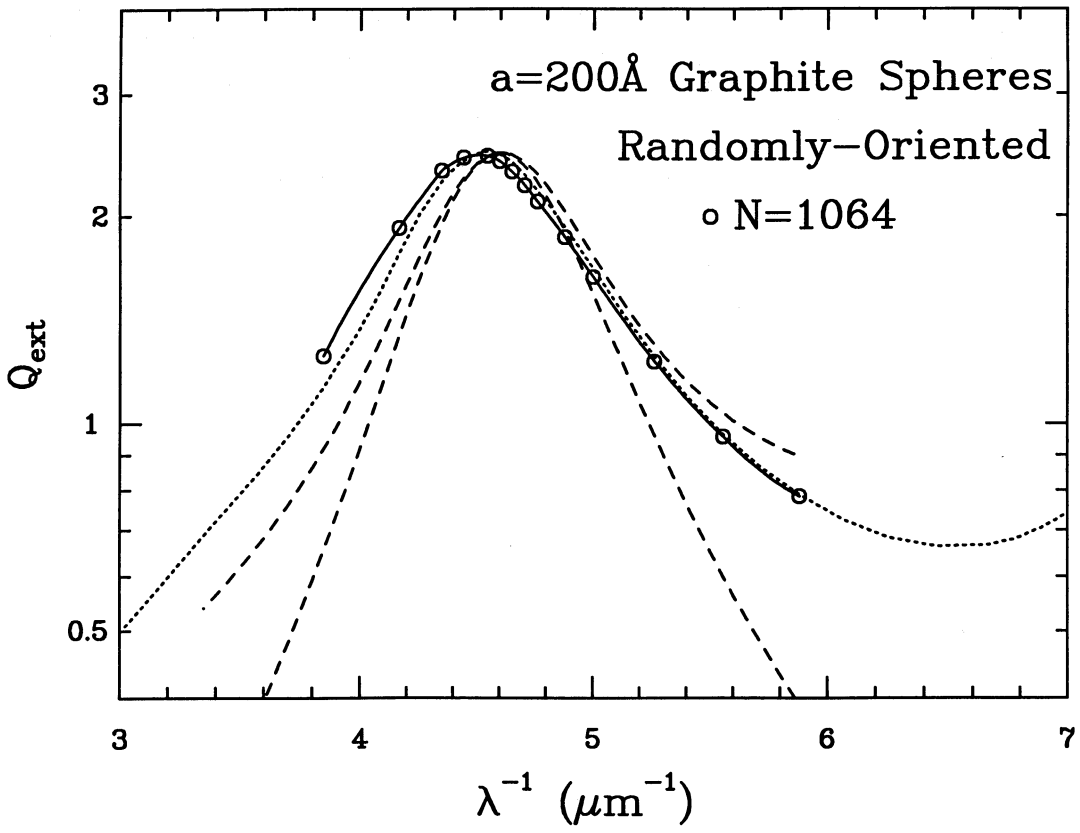

FIG. 7*a*

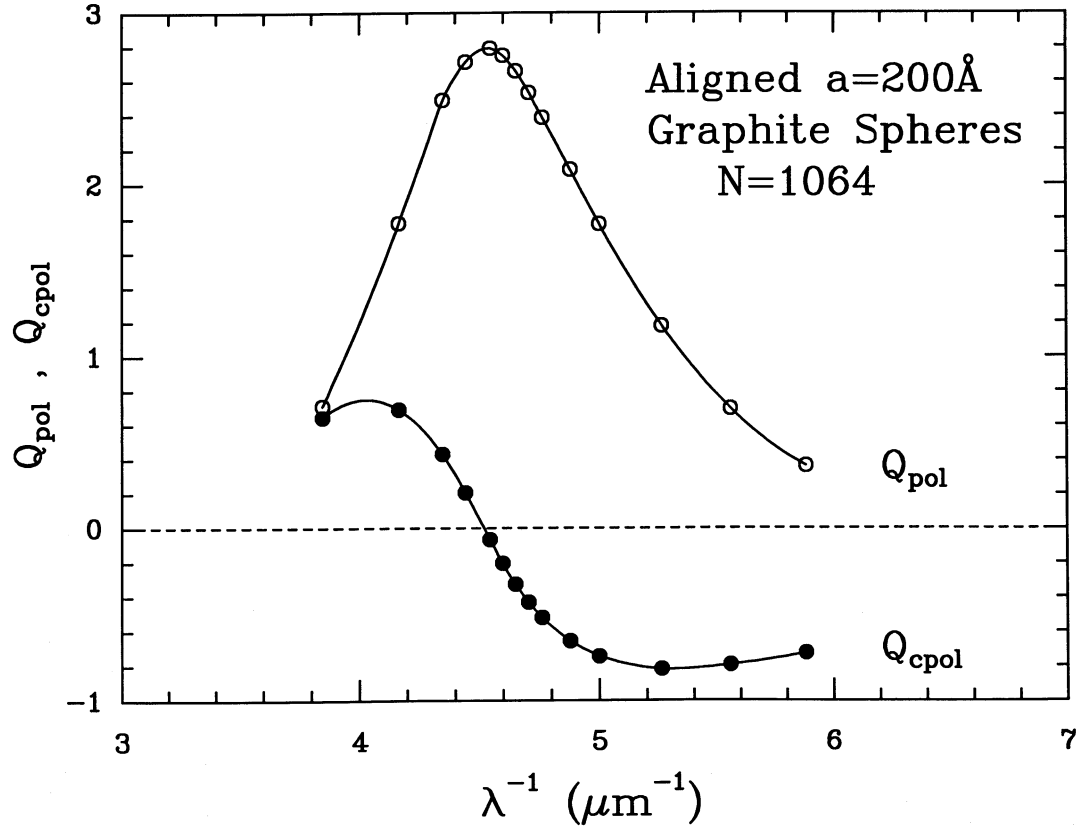

FIG. 7*b*

FIG. 7.—(*a*) Same as Fig. 6*a*, but for $a = 200$ Å, with $\lambda_{ext,max} \approx 4.65\ \mu m^{-1}$. (*b*) Same as Fig. 6*b*, but for $a = 200$ Å; $\lambda^{-1}_{pol,max} \approx 4.53\ \mu m^{-1}$, and $\lambda_c^{-1} \approx 4.52\ \mu m^{-1}$.

have minimum free energy when they have a flattened, flake-like, geometry, with the graphite c-axis normal to the flattening plane.[6] However, under some growth conditions screw dislocations can lead to the formation of graphite "whiskers," with the graphite c-axis parallel to the axis of the whisker.

Gilra (1971) has discussed the optical properties of small graphite particles. Gilra made several points: (1) Very small graphite spheres have an extinction peak shortward of 2175 Å, but this peak shifts to longer wavelengths as the particle size is increased, and coincides with the observed peak for $a \approx 150$ Å; (2) The extinction peak shifts to longer (or shorter) wavelengths for oblate (or prolate) spheroidal shapes (taking the spheroid symmetry axis to coincide with the graphite c-axis); (3) The extinction peak would be appreciably shifted to longer wavelengths if the graphite grains were coated with a dielectric substance (e.g., ice). Gilra concluded from the above results that if graphite was responsible for the observed 2200 Å extinction bump, then the graphite particles producing this feature should be approximately spherical, and should have $a \approx$ 150 Å. Gilra also concluded that interstellar graphite grains could have essentially no coating; however, Hecht (1981) subsequently showed that small graphite spheres with appreciable ice coatings cannot be excluded. Since it is widely appreciated that crystalline graphite particles would be unlikely to be spherical, Gilra's conclusions regarding shape have been sometimes used to argue that the observed 2175 Å feature is unlikely to be due to graphite (even though Gilra himself concluded that "the 2200 Å interstellar band is very likely due to graphite particles").

Gilra's and Hecht's results were based on approximate calculations. The results for bare and coated spheres were based on the "$\frac{1}{3}$–$\frac{2}{3}$" approximation; we have seen above that this approximation is surprisingly accurate for $a \lesssim 200$ Å, and therefore should not compromise either Gilra's result for the size dependence of the extinction peak for graphite spheres nor the conclusions of Gilra and Hecht regarding the effects of coatings on the position of the extinction peak. The results for nonspherical graphite grains were based on calculations valid for ellipsoids in the "Rayleigh limit." Since for graphite particles and $\lambda \approx 2200$ Å the Rayleigh limit is valid only for $a \lesssim$ 50 Å, it is not clear how Gilra's results for ellipsoidal graphite grains may be modified for $a_{eq} \gtrsim 50$ Å. Furthermore, since graphite particles are just as unlikely to form ellipsoids as they are to form spheres, it is of interest to consider other shapes.

Discrete-dipole calculations have therefore been carried out for three different graphite grain shapes, shown in Figure 8. The three arrays considered are all approximations to cylinders, with varying axis ratios. The cylinder length is $2a$, the diameter is $2b$, and the "equivalent radius" is $a_{eq} = (3ab^2/2)^{1/3}$. We first consider a flattened disk with a 3:1 aspect ratio ($N = 480$, $b/a = 3.090$); this represents the graphite "flake" geometry suggested by thermodynamic considerations. In addition to the 3:1 disk, we consider a less-flattened 1.5:1 disk ($N = 960$, $b/a = 1.545$), as well as a 1.5:1 "rod" ($N = 624$, $a/b = 1.475$). In each case it is assumed that the graphite is oriented with the c-axis parallel to the axis of the cylinder. For each array and each wavelength, we performed scattering calculations for three special geometries: (1) $\boldsymbol{k}$ along the cylinder axis; (2) $\boldsymbol{k}$ perpendicular to the axis, $\boldsymbol{E}$ parallel to the axis; (3) $\boldsymbol{k}$ perpendicular to the axis, $\boldsymbol{E}$ perpendicular to the axis. To estimate the extinction for a randomly-oriented ensemble, we took the average of the three extinction cross sections; this is exact only in the "electric dipole" limit, but is expected to provide a good approximation. (Calculation of the scattering properties for other incidence angles would have been extremely time consuming, since those geometries lack the fourfold symmetry of the three special geometries considered above and, for a fixed N, the time required to obtain a solution increases by about a factor of 10 when fourfold symmetry cannot be assumed.)

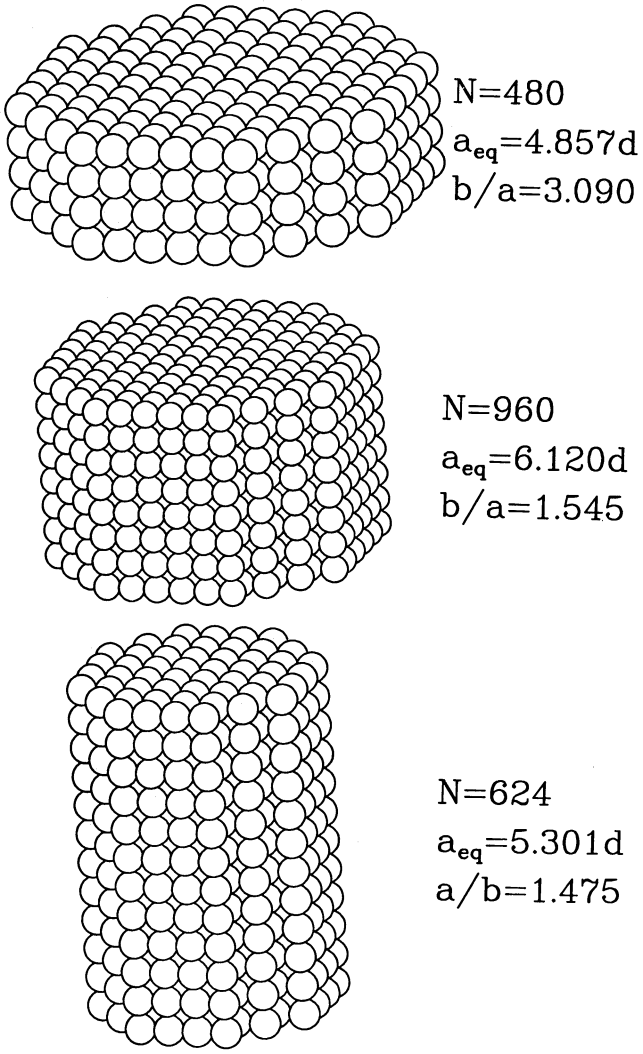

FIG. 8.—(*a*) $N = 480$ finite-element representation of a "disk" with $b/a = 3.090$; (*b*) $N = 960$ representation of a "disk" with $b/a = 1.545$; (*c*) $N = 624$ representation of a "rod" with $a/b = 1.475$.

The results for the 3:1 flattened disk are shown in Figures 9, 10, and 11, for $a_{eq} = 50$, 100, and 200 Å. Just as found by Gilra for small oblate spheroids with appreciable flattening, the $a_{eq} = 50$ Å 3:1 disk has the extinction peak occurring appreciably longward of the observed peak at 2175 Å. Note that the extinction peak shifts longward slightly in going from $a_{eq} = 50$ Å to 100 Å, indicating that the $a_{eq} = 100$ Å case is no longer

[6] If the surface free energies σ_1 and σ_2 apply to the basal plane and "sides," respectively, then the cylindrical shape minimizing the surface free energy has an aspect ratio (diameter/length) $b/a = \sigma_2/\sigma_1$. The surface free energies of graphite are not well determined, but a ratio $\sigma_2/\sigma_1 \approx 2$–3 is not unreasonable.

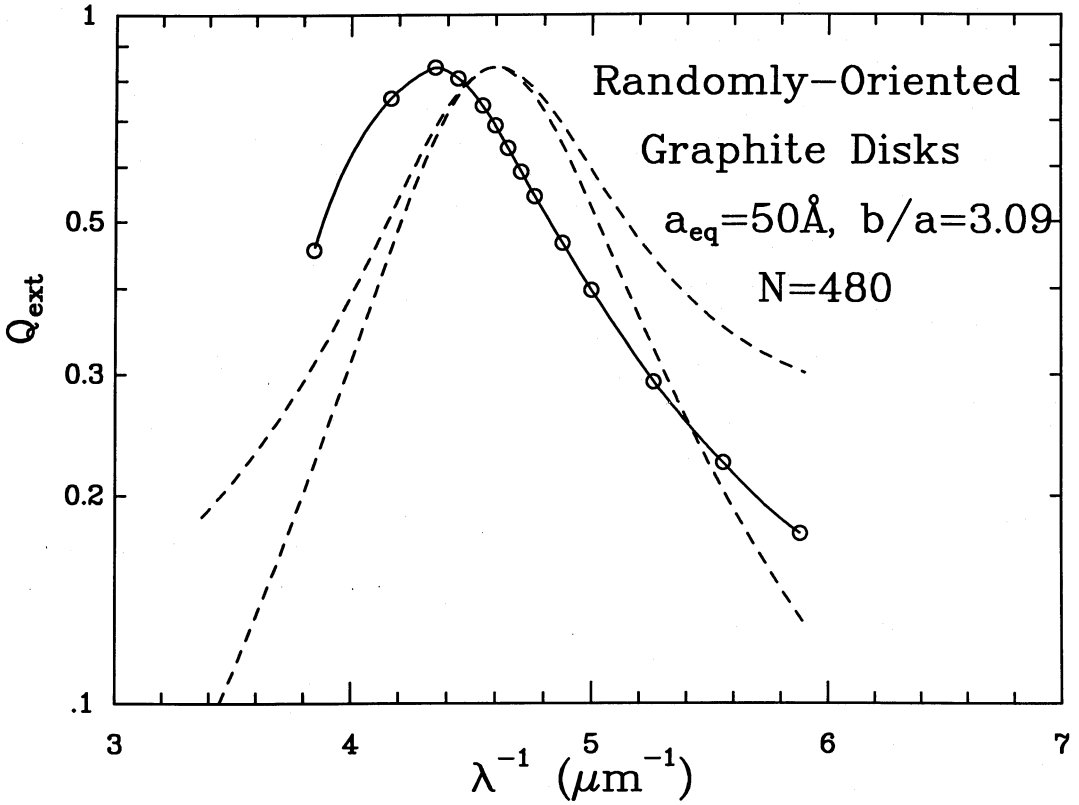

FIG. 9.—(*a*) Extinction cross sections for randomly oriented 3.09:1 graphite disks with a_{eq} = 50 Å, approximated by an N = 480 element dipole array (see Fig. 7*a*). The extinction peak is at $\lambda^{-1}_{ext,max} \approx 4.34\ \mu m^{-1}$, significantly shortward of the observed value of 4.6 μm^{-1}. Also plotted (*dashed lines*) are the analytic fits by Fitzpatrick and Massa (1986) for the 3.35–5.9 μm^{-1} extinction, for 0.0 and 0.25 of the mean linear contribution (see text). It is evident that the observed extinction bump cannot be due to these particles.

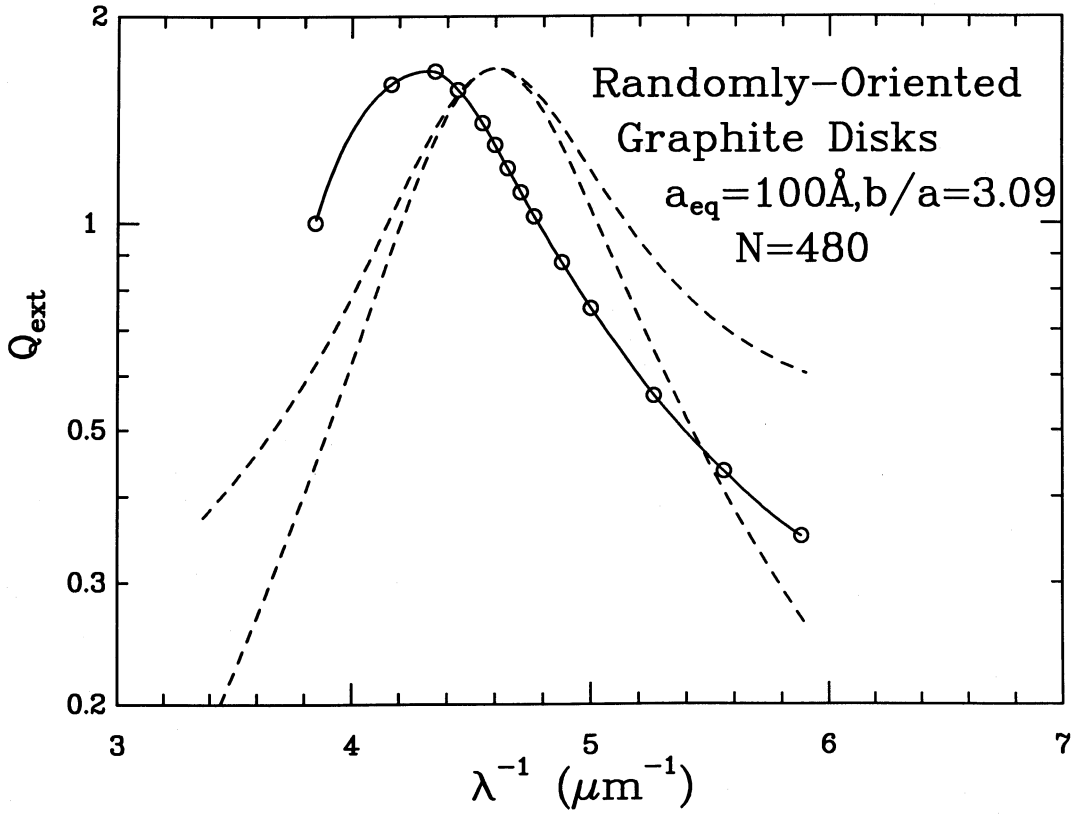

FIG. 10.—Same as Fig. 9, but for a_{eq} = 100 Å, for which $\lambda^{-1}_{ext,max} \approx 4.30\ \mu m^{-1}$. Comparison with Fig. 9 shows that increasing the particle size from a_{eq} = 50 Å to a_{eq} = 100 Å resulted in a slight shift in the extinction peak to shift to longer wavelengths.

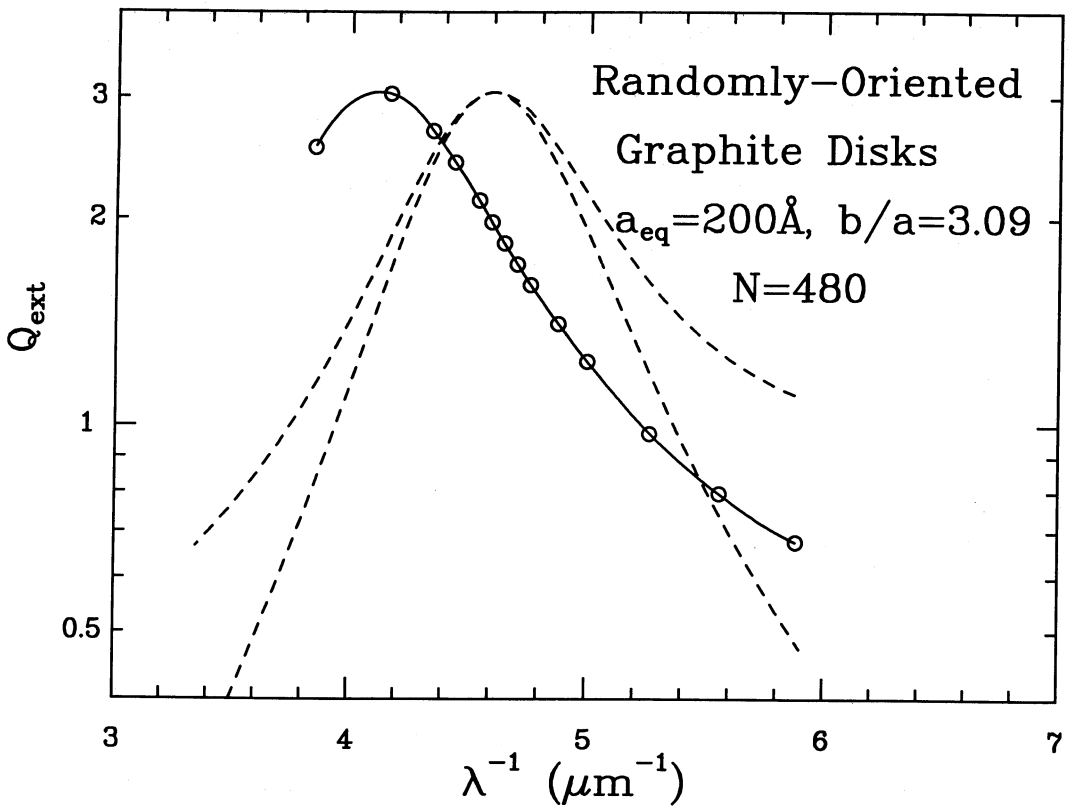

FIG. 11.—Same as Fig. 9, but for $a_{eq} = 200$ Å, for which $\lambda^{-1}_{ext,max} \approx 4.12\ \mu m^{-1}$

strictly in the electric dipole limit. A substantial shift to longer wavelengths occurs in going from $a_{eq} = 100$ Å to $a_{eq} = 200$ Å. It is evident that the interstellar grain population cannot contain an appreciable quantity of graphite in such a flattened geometry.

As shown in Figure 12, however, the slightly flattened 1.5:1 disk with $a_{eq} = 100$ Å has an extinction peak which coincides fairly closely with the observed interstellar feature, although the width of the feature requires that an appreciable fraction of the continuum extinction be associated with the feature. The agreement would be similar for grain sizes $a_{eq} < 100$ Å, since, as seen in Figures 9 and 10, one is just beginning to leave the "electric dipole" limit at $a_{eq} \approx 100$ Å. Thus 1.5:1 disks with $a_{eq} \lesssim 100$ Å could contribute appreciably to the observed interstellar 2175 Å feature. However, Figure 13 shows that increasing the size of the 1.5:1 disk to $a_{eq} = 200$ Å results in an appreciable shift in the peak to longer wavelengths; this case is sufficiently unlike the observed interstellar feature that one can conclude that 1.5:1 disks with $a_{eq} \approx 200$ Å cannot make an appreciable contribution to the extinction at these wavelengths.

Turning to the 1.5:1 "rod," we see from Figure 14 that small $a_{eq} \lesssim 100$ Å particles of this shape produce an extinction feature peaking at too short a wavelength. If, however, the size is increased to $a_{eq} \approx 200$ Å, the feature shifts so that the peak coincides fairly well with the observed 2175 Å feature (see Fig. 15), although the computed profile does not fall off quite rapidly enough at long wavelengths. Evidently 1.5:1 $a_{eq} \approx 200$ Å rods could contribute part of the observed extinction at 2175 Å, but would have to be mixed with other grains (other graphite shapes and sizes) having a narrower extinction profile, in order for the composite profile to agree with the observations. From the above we conclude that the 2175 Å feature could be due to small ($a_{eq} \lesssim 200$ Å) graphite particles; the particles need not be spherical, but should have aspect ratios not differing greatly from unity.

The hypothesis that the 2175 Å feature is produced by small graphite grains is strongly challenged by the results of the observational study by Fitzpatrick and Massa (1986); they found that the wavelength λ_{peak} at which the feature peaks is nearly invariant among the 45 lines of sight which they studied, whereas the FWHM (full width at half-maximum) of the feature showed significant variation. (Overall, neither λ_{peak} nor the FWHM varied greatly: more than half of the lines of sight had λ^{-1}_{peak} within $\pm 0.32\%$ of 4.594 μm^{-1}, and more than half had FWHM within $\pm 5.7\%$ of 0.984 μm^{-1}.) Furthermore, no correlation between λ_{peak} and FWHM was evident. Since λ_{peak} is quite sensitive to particle sizes, shapes, and coatings, the graphite hypothesis appears to require that the size and shape distributions of the $a \lesssim 300$ Å graphite particles vary little from one line of sight to another, and that coatings be either constant or absent; if so, however, it is not clear what mechanism is to account for the observed variation in FWHM. Since we have seen that the graphite grains with 1:1 axial ratios have peaks at ~ 2175 Å, perhaps the variable width of the feature could be attributed to variable admixtures of particles with axial ratios other than 1:1, in order to hold the peak position constant, such admixtures would have to contain roughly equal proportions of flattened and elongated particles, a restriction which makes this explanation appear somewhat unnatural. However, it should be noted that *all* of the hypotheses for the 2175 Å feature lack a "natural" means for varying

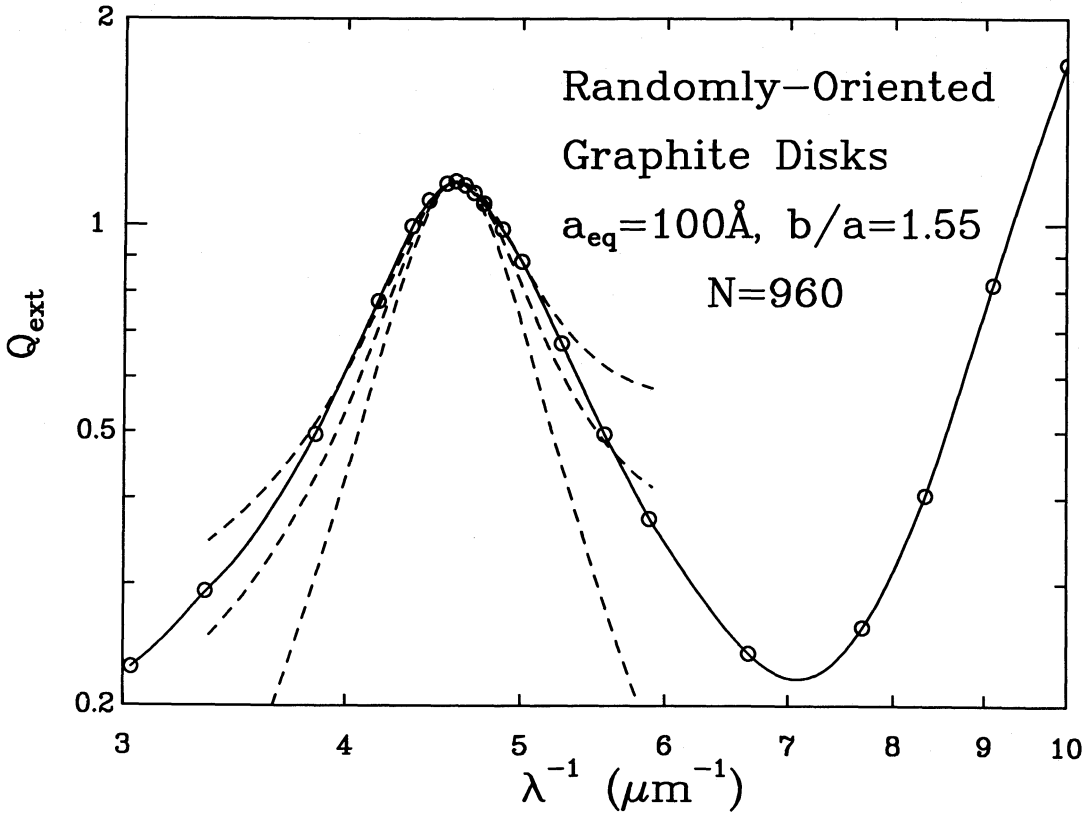

FIG. 12.—Same as Fig. 9, but for 1.5:1 graphite disks with a_{eq} = 100 Å, for which $\lambda^{-1}_{ext,max} \approx 4.59\ \mu m^{-1}$. Three fits (Fitzpatrick and Massa 1986) to the observed extinction feature are shown, plus 0.0, 0.25, and 0.5 of the mean linear contribution (see text). These 1.5:1 disks may be consistent with the observed extinction profile.

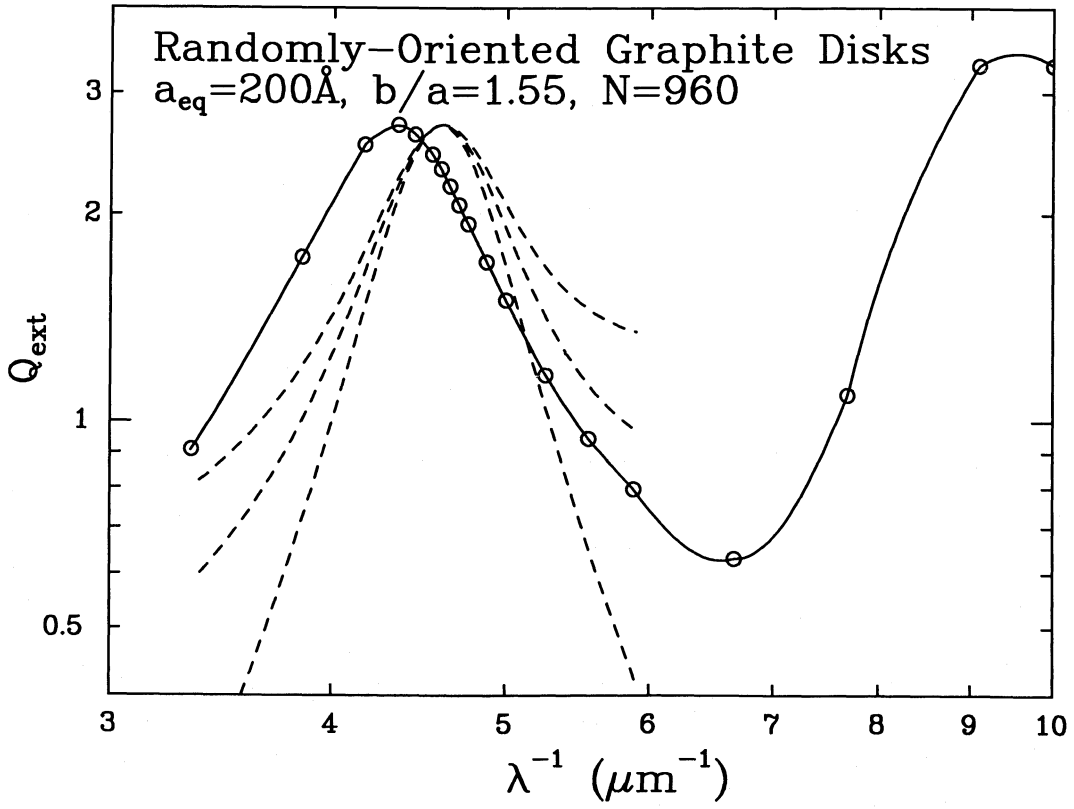

FIG. 13.—Same as Fig. 12, but for 1.5:1 graphite disks with a_{eq} = 200 Å, for which $\lambda^{-1}_{ext,max} \approx 4.35\ \mu m^{-1}$; comparison with Fig. 12 shows that the increase in particle size led to a significant shift in the peak to longer wavelengths. Such particles appear to be inconsistent with the observed extinction profile.

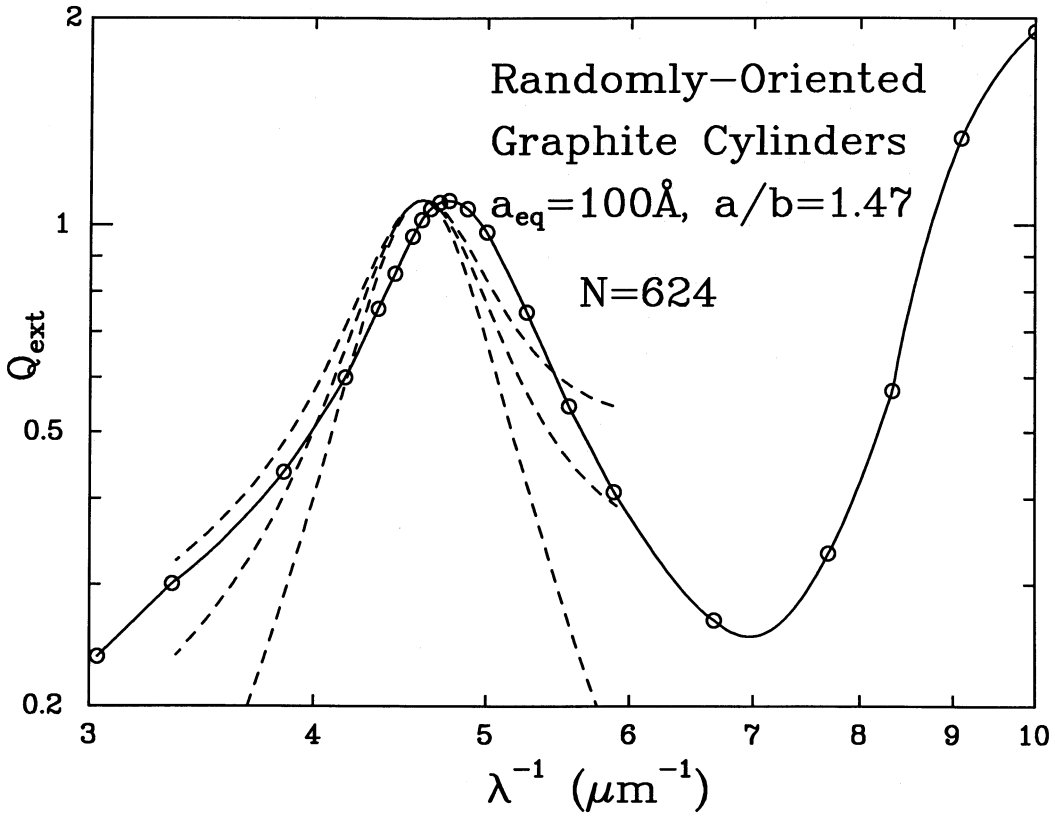

FIG. 14.—Same as Fig. 12, but for 1.5:1 graphite rods with a_{eq} = 100 Å, for which $\lambda^{-1}_{ext,max} \approx 4.76\ \mu m^{-1}$. The peak occurs appreciably shortward of the observed profile.

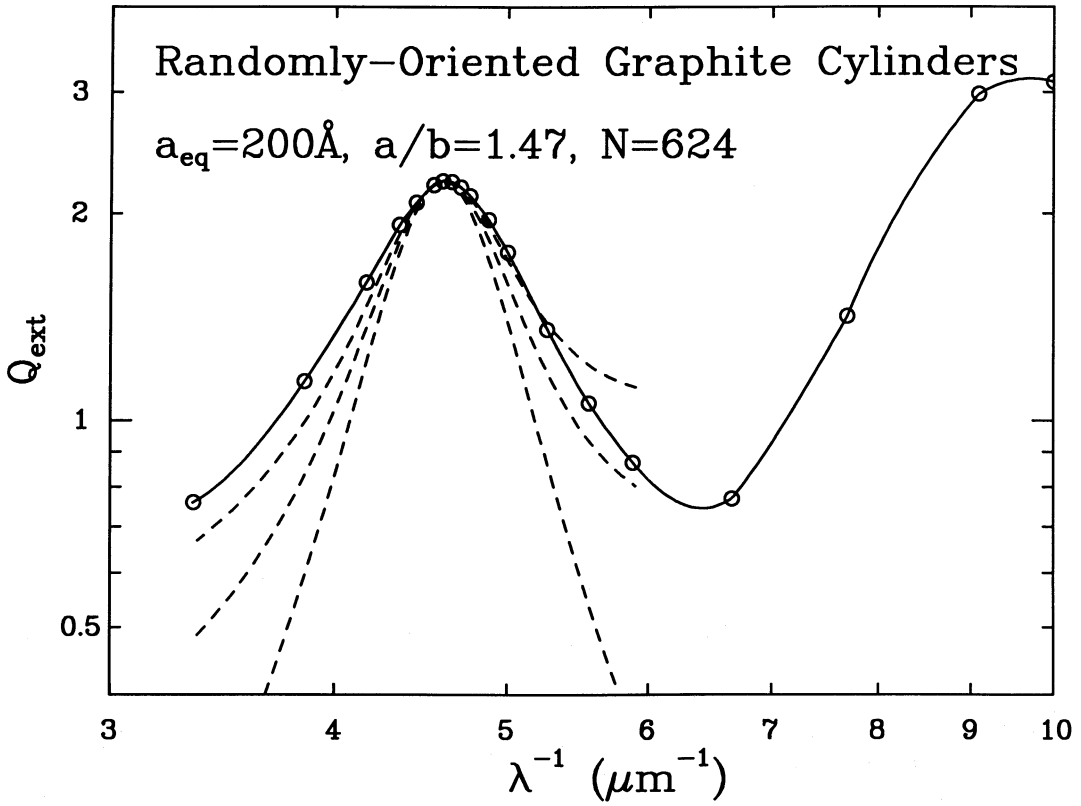

FIG. 15.—Same as Fig. 12, but for 1.5:1 graphite rods with a_{eq} = 200 Å, for which $\lambda^{-1}_{ext,max} \approx 4.61\ \mu m^{-1}$. Comparison with Fig. 14 shows that the increase in particle size shifted the peak to longer wavelengths, bringing it into approximate agreement with the observed profile, although it appears to be somewhat too broad on the long-wavelength side of the feature.

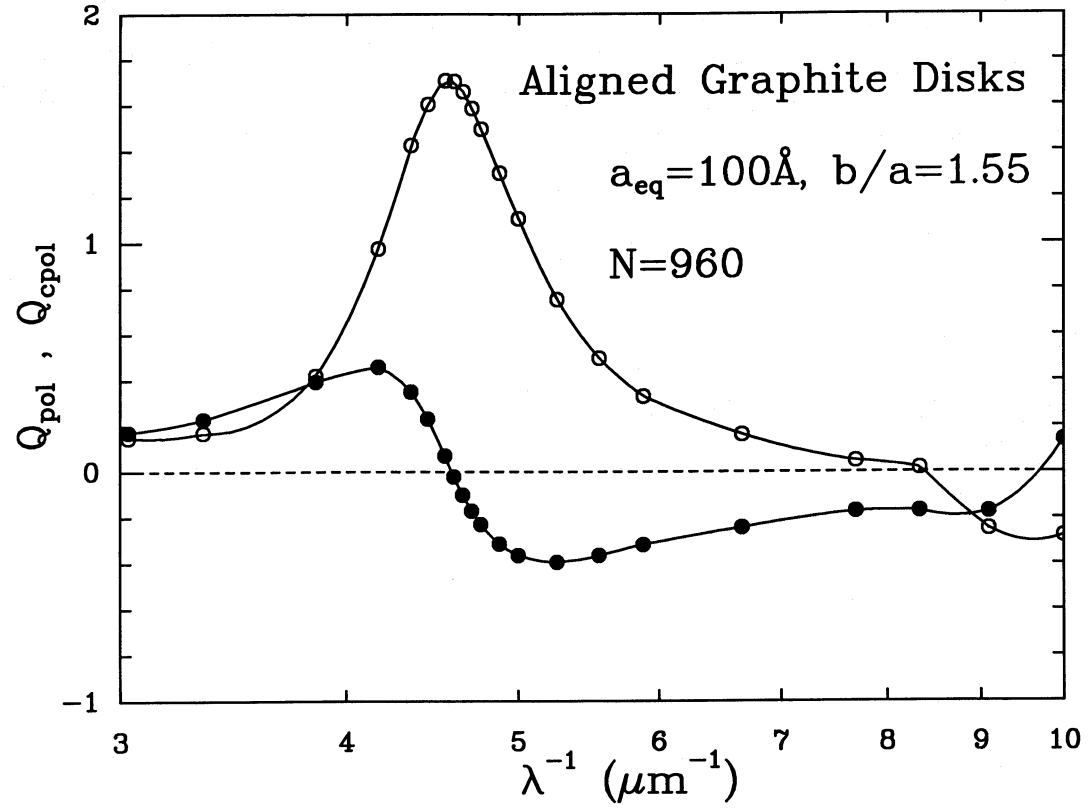

FIG. 16*a*

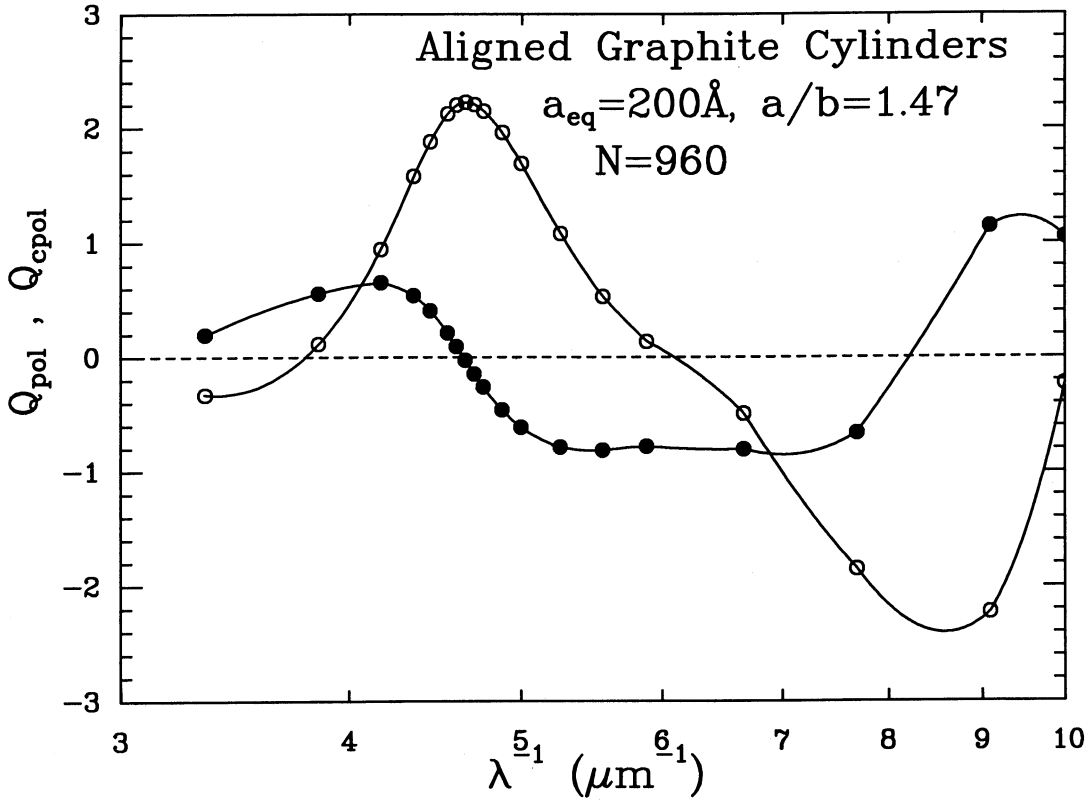

FIG. 16*b*

FIG. 16.—Linear and circular polarization cross efficiency factors for the two cylindrical graphite particles which appeared to be consistent with the observed 2175 Å extinction feature: (*a*) 1.5:1 graphite disk, with a_{eq} = 100 Å, for which the linear polarization peak occurs at $\lambda_{pol,max} \approx 4.57$ μm^{-1}, and the circular polarization crossover occurs at $\lambda_c \approx 4.59$ μm^{-1}. Spinning alignment of these disks would lead to a linear polarization peak with the same direction as the linear polarization at visual wavelengths. (*b*) 1.5:1 graphite rod, with a_{eq} = 200 Å, for which the linear polarization peak occurs at 4.65 μm^{-1}, and the circular polarization crossover occurs at $\lambda_c \approx 4.64$ μm^{-1}. Spinning alignment of these rods would lead to a linear polarization contribution near the peak which is orthogonal to the linear polarization at visual wavelengths, and effective efficiency factors reduced by a factor of 2 below the value plotted here. Note that the linear and circular polarization efficiencies at $\lambda^{-1} \gtrsim 6$ μm^{-1} differ appreciably from those for the 1.5:1 graphite disk.

the width of the feature while holding the central position constant, so that the graphite hypothesis cannot be rejected on this basis.

Having seen that two of the graphite grain geometries examined here may be consistent with the observed 2175 Å extinction feature, we now consider what polarization of starlight would result if such grains were partially aligned. In Figure 16 we show the linear and circular polarization efficiencies for perfectly aligned grains of the two types considered. The first point to note is that both the $a_{eq} = 100$ Å 1.5:1 disk and the $a_{eq} = 200$ Å 1.5:1 rod, if aligned, are very efficient polarizers in the neighborhood of the 2175 Å extinction peak. The second point to note is that both of these grains have circular polarization "crossover" wavelengths which are nearly identical to the wavelengths of peak linear polarization. The third point to note is that the linear (and circular) polarization cross sections of the grains, while similar in the neighborhood of the extinction peak, differ greatly at wavelengths $\lambda \lesssim 1700$ Å. This is because near 2200 Å graphite absorption is far stronger for $E \perp c$ than for $E \parallel c$, and hence the 2200 Å feature is associated with the polarization state perpendicular to the cylinder axis. At shorter wavelengths, however, graphite becomes strongly absorbing for both polarization states, and in fact has a strong absorption "feature" at ~ 950 Å associated with the $E \parallel c$ component of the dielectric tensor. Since elongation along the c-axis enhances the efficacy of the $E \parallel c$ absorption, and reduces the efficacy of the $E \perp c$ absorption, it follows that the relative strengths of the absorption at 2200 and 1000 Å depend upon the grain shape: rods have larger values of the ratio Q_{ext}(1000 Å)/Q_{ext}(2200 Å) than do disks. Furthermore, since these two absorption features are associated with orthogonal polarization states, it follows that the linear polarization profile differs greatly between disks and rods, with the rods tending to have strong 1000 Å polarization opposite in "sign" to the 2200 Å polarization.

We draw the following conclusions: If the 2175 Å feature is due to graphite particles, and *if* those particles are partially aligned, then (i) There should be a strong linear polarization feature near 2175 Å; (ii) For "spinning" grain alignment, the "sense" of the 2175 Å feature depends upon the grain shape: for "flakes" the sense is the same as the polarization at visual wavelengths, while for "rods" the sense is opposite; (iii) Rod-shaped grains should produce a strong polarization feature near 1000 Å (with a "normal" sense of polarization), whereas disk-shaped grains tend to contribute relatively weak polarization near 1000 Å.

To date there have only been very limited observations of the ultraviolet linear polarization, consisting of broad-band observations from a balloon at 2860 Å and 2250 Å for ζ Oph, and observations at 2250 Å for κ Cas (Gehrels 1974). Unfortunately, all that can be concluded from these observations is that any 2175 Å polarization feature is not extremely strong. When orbited, WUPPE (Wisconsin Ultraviolet Photo Polarimeter Experiment) on the Space Shuttle and the FOS (Faint Object Spectrograph) on the Hubble Space Telescope will permit sensitive linear and circular polarimetry in the ultraviolet. If no 2175 Å linear polarization feature is detected, it will rule out the presence of small aligned graphite grains. If polarization in the 2175 Å feature is detected, then the "sense" of the excess polarization, as well as observations of the linear polarization near 7.7 μm^{-1} (maximum λ^{-1} for *WUPPE*), may serve to discriminate between flattened or elongated graphite grains.

IX. SUMMARY

1. The Discrete Dipole Approximation (DDA) is a flexible tering of radiation by particles of arbitrary shape. The method has been extended to incorporate the effects of radiative reaction and to allow for possible anisotropy of the dielectric tensor of the material.

2. Formulae are given for the evaluation of extinction, absorption, scattering, and polarization cross sections once the dipole polarizations have been obtained.

3. A simple numerical algorithm based on the method of conjugate gradients is found to provide an efficient and robust method for obtaining accurate solutions to the scattering problem. The method works well for absorptive, as well as dielectric, grain materials.

4. The validity of the DDA is examined, and it is found that both magnetic dipole effects and "edge" effects can limit the accuracy of the method for materials with large dielectric constants. Two validity criteria must be satisfied: in order that its shape be adequately represented, the number N of dipoles must exceed N_{min} given by equation (4.01). If $N > N_{min}$, then the dipole array will provide a satisfactory approximation provided $ka_{eq} < ka_{crit}$, where ka_{crit} is given by equation (4.05).

5. The accuracy of the DDA is verified by comparison of DDA calculations for spheres with exact results from Mie theory.

6. The DDA is used to compute extinction cross sections for spherical graphite grains of radii $a = 100$ Å and 200 Å. The often-used "$\frac{1}{3}$–$\frac{2}{3}$" approximation is found to be surprisingly accurate, at least for these grain sizes.

7. The DDA is used to calculate extinction cross sections for nonspherical graphite grains with three different geometries. On the basis of comparison with the mean observed interstellar 2175 Å extinction profile, it is concluded that the observed interstellar feature *could* be produced by small graphite grains which need not be spherical, but which should have aspect ratios not differing greatly from unity. In particular, slightly flattened 1.5:1 "disks" with equivalent radii $a_{eq} \lesssim 100$ Å fit the observed feature fairly well

8. Linear and circular polarization cross sections are calculated for nonspherical graphite grains. Small graphite particles have distinct, shape-dependent linear and circular polarization cross sections. If the interstellar 2175 Å feature is due to graphite, and if these graphite grains are appreciably aligned, then measurements of the linear and circular polarization in the ultraviolet may be used to discriminate among different grain models.

I wish to thank Y. L. Yung for referring me to the literature on conjugate gradient methods. I also wish to thank E. Fitzpatrick, P. Flatau, P. G. Martin, M. H. Lee, E. M. Purcell, L. Spitzer, Jr., R. West, and E. L. Wright for helpful comments. This research was supported in part by grants AST-8341412 and AST-8612013 from the National Science Foundation.

REFERENCES

Asano, S. 1979, *Appl. Optics*, **18**, 716.
Asano, S., and Sato, M. 1980, *Appl. Optics*, **19**, 962.
Asano, S., and Yamamoto, G. 1975, *Appl. Optics*, **14**, 29.
Barber, P., and Yeh, C. 1975, *Appl. Optics*, **14**, 2684.
Bohren, C. F., and Huffman, D. R. 1983, *Absorption and Scattering of Light by Small Particles* (New York: Wiley).
Carnochan, D. J. 1986, *M.N.R.A.S.*, **219**, 903.
Debye, P. 1909, *Ann. Phys.*, **30**, 57.
Draine, B. T. 1985, *Ap. J. Suppl.*, **57**, 587.
Draine, B. T., and Lee, H. M. 1984, *Ap. J.*, **285**, 289.
Druger, S. D., Kerker, M., Wang, D.-S., and Cooke, D. D. 1979, *Appl. Optics*, **18**, 3888.
Fitzpatrick, E. L., and Massa, D. 1986, *Ap. J.*, **307**, 286.
Gehrels, T. 1974, *A.J.*, **79**, 590.
Gilra, D. P. 1972, in *The Scientific Results of OAO-2*, ed. A. D. Code (NASA SP310), p. 295.
Haracz, R. D., Cohen, L. D., and Cohen, A. 1984, *Appl. Optics*, **23**, 436.
———. 1985, *Appl. Phys.*, **58**, 3322.
Hecht, J. 1981, *Ap. J.*, **246**, 794.
Jackson, J. D. 1975, *Classical Electrodynamics* (2d ed., New York: Wiley).
Kattawar, G. W., and Humphreys, T. J. 1980, in *Light Scattering by Irregularly Shaped Particles*, ed. D. W. Schuerman (New York: Plenum), p. 177.
Kittel, C. 1971, *Introduction to Solid State Physics* (4th ed.; New York: Wiley).
Martin, P. G. 1972, *M.N.R.A.S.*, **153**, 179.
———. 1975*a*, *Ap. J.*, **201**, 373.
———. 1975*b*, *Ap. J.*, **202**, 389.
Mie, G. 1908, *Ann. Phys.*, **25**, 377.
Onaka, T. 1980, *Ann. Tokyo Astr. Obs.*, **18**, 1.
Petravic, M., and Kuo-Petravic, G. 1979, *J. Comput. Phys.*, **32**, 263.
Press, W. H., Flannery, B. P., Teukolsky, S. A., and Vetterling, W. T. 1986, *Numerical Recipes* (Cambridge: Cambridge University Press).
Purcell, E. M. 1965, *Electricity and Magnetism, Berkeley Physics Course*, Vol. **1** (1st ed.; New York: McGraw-Hill).
Purcell, E. M., and Pennypacker, C. R. 1973, *Ap. J.*, **186**, 705.
Savage, B. D. 1975, *Ap. J.*, **199**, 92.
Shapiro, P. R. 1975, *Ap. J.*, **201**, 151.
Singham, S. B., and Bohren, C. F. 1987, *Opt. Letters.*, **12**, 10.
Wiscombe, W., and Mugnai, A. 1980, in *Light Scattering by Irregularly Shaped Particles*, ed. D. W. Schuerman (New York: Plenum), p. 141.
Wright, E. L. 1987, *Ap. J.*, **320**, 818.
Yeh, C., and Mei, K. K. 1980, in *Light Scattering by Irregularly Shaped Particles*, ed. D. W. Schuerman (New York: Plenum), p. 201.
Yung, Y. L. 1978, *Appl. Optics*, **17**, 3707.

B. T. DRAINE: Peyton Hall, Princeton University, Princeton, NJ 08544